Aus dem Biomedizinischen Zentrum
Institut für Chirurgische Forschung
der Ludwig-Maximilians-Universität München
Kommissarischer Direktor: Prof. Dr. med. dent. Reinhard Hickel
und
aus der Klinik und Poliklinik für Hals-Nasen-Ohrenheilkunde
der Ludwig-Maximilians-Universität München
Direktor: Prof. Dr. med. Martin Canis

In vivo assessment of hair cell toxicity of gadolinium-based contrast agents in *Xenopus* embryos

Mit Genehmigung der Medizinischen Fakultät

der Universität München

Berichterstatter: Prof. Dr. André W. Brändli

Mitberichterstatter: Prof. Dr. Olaf Dietrich

PD Dr. Jesus Bujia

Dekan: Prof. Dr. med. dent. Reinhard Hickel

Tag der mündlichen Prüfung: 17.01.2019

Eidesstattliche Versicherung

Eichel, Vanessa

Name, Vorname

Ich erkläre hiermit an Eides statt, dass ich die vorliegende Dissertation mit dem Thema:

In vivo assessment of hair cell toxicity of gadolinium-based contrast agents in *Xenopus* embryos

selbständig verfasst, mich außer der angegebenen keiner weiteren Hilfsmittel bedient und alle Erkenntnisse, die aus dem Schrifttum ganz oder annähernd übernommen sind, als solche kenntlich gemacht und nach ihrer Herkunft unter Bezeichnung der Fundstelle einzeln nachgewiesen habe.

Ich erkläre des Weiteren, dass die hier vorgelegte Dissertation nicht in gleicher oder in ähnlicher Form bei einer anderen Stelle zur Erlangung eines akademischen Grades eingereicht wurde.

Heidelberg, 17.01.2019   Vanessa Eichel

Ort, Datum   Unterschrift Doktorand

to my parents Margit and Hans Werner

CONTENTS

ABSTRACT

Meniere´s disease (MD) is a disorder of the inner ear causing episodic attacks of vertigo, hearing loss, and tinnitus. An inner ear magnetic resonance imaging (MRI) method was introduced in 2007, which enables the visualization of the endolymphatic hydrops, an important pathologic feature of MD. The method is usually performed by applying gadolinium-based contrast agents (GBCAs) intratympanically and at significant lower doses as compared to the intravenous enhanced doses. The procedure has provided important insights into the pathophysiology of MD and has become a standard procedure for the diagnosis of the disease. Various GBCAs have been used, but the potential toxicities towards sensory hair cells of the inner ear are still poorly understood.

In the present work a standardized *in vivo* 24-hour test assay was employed for the quantitative assessment of the toxicities of the major GBCAs towards hair cells of the lateral line system of *Xenopus* embryos. After compound treatment, the hair cells were stained fluorescently with the dye FM1-43FX and the fluorescence intensity was quantitated by fluorescence microscopy. Five commonly used gadolinium-based contrast agents, Gadodiamide (Omniscan®), gadobutrol (Gadovist®), gadobenate dimeglumine (MultiHance®), gadoterate meglumine (Dotarem®), and gadopentetate dimeglumine (Magnograf® or Magnevist®) were assessed. They represent all four different types of GBCAs based on the type of ligand (linear or macrocyclic) and charge (ionic or non-ionic).

Dose-response studies were carried out to determine EC_{50} values (effective concentration reducing hair cells staining to 50%) for each GBCA. Free gadolinium served as a baseline and was toxic to hair cells with an EC_{50} of 9.7 µM. By contrast, the non-ionic Omniscan and Gadovist displayed no significant hair cell toxicities over the entire concentration range (1 – 100 mM) tested. The other GBCAs, all of the ionic class, showed increasing hair cell toxicity with relative fluorescence units decreasing below 75% at 50 mM. Interestingly, MultiHance, and Magnograf were found to be lethal to *Xenopus* embryos at concentrations of 100 mM. Therefore, the potential adverse effects of GBCA treatment on *Xenopus* embryogenesis were investigated in greater detail by

monitoring embryos over a five-day period. Free gadolinium caused lethality to 50% of the embryos (LC_{50}) at an estimated concentration of 56.7 µM. Embryonic lethality was also observed with the ionic MultiHance, Magnograf, and Dotarem, but the estimated LC_{50} values ranged between 50 and 110 mM. By contrast, treatments with the non-ionic Omniscan and Gadovist did not interfere with *Xenopus* embryogenesis even at 100 mM, the highest concentration tested. While ionicity was important determinant for hair cell toxicity and embryonic lethality of GBCAs, ligand structure (linear or macrocyclic) was less critical.

On the basis of the *Xenopus* tests, the following conclusions were made. The importance of stable chelation of gadolinium was underlined by the high toxicity of free gadolinium towards *Xenopus* embryos and the hair cells of the lateral line. Hair cell toxicity of GBCAs, particularly for those of the non-ionic type, was minimal at concentrations typically used for intratympanic administration in MD diagnosis, suggesting that these GBCAs are safe for MR imaging. The recent European Medicines Agency (EMA) recommendations to suspend the use of the linear GBCAs Omniscan, MultiHance, and Magnograf, mainly due to the higher risk of retention in human body, underlines the importance of low-dose applications as practiced in the intratympanic enhanced MRI method. Among the five GBCAs tested in *Xenopus* embryos, the non-ionic Omniscan and Gadovist showed the best safety profiles. However, the higher deposition-rate of Omniscan in the human body favors the use of Gadovist for intratympanic application.

ZUSAMMENFASSUNG

Morbus Ménière ist eine Erkrankung des Innenohrs die Schwindelattacken, Hörverlust und Tinnitus verursachen kann. Im Jahre 2007 wurde eine neue Innenohr-MRT-Methode eingeführt, die es ermöglicht den endolymphatischen Hydrops (EH), eine wichtige Pathologie des Morbus Ménière, darzustellen. Bei diesem Verfahren werden Gadolinium-basierte Kontrastmittel intratympanal appliziert. Die lokal verstärkte Innenohr-MRT hat zu neuen pathophysiologischen Erkenntnissen geführt und ist zu einem wichtigen diagnostischen Nachweisverfahren für Morbus Ménière geworden. Es werden verschiedene Gadolinium-basierte Kontrastmittel eingesetzt, deren mögliche Toxizität für die Haarzellen des Innenohrs jedoch bisher unvollständig untersucht wurde.

In der vorliegenden Arbeit wurde die Toxizität der wichtigsten Kontrastmittel für die Haarzellen der Seitenlinienorgane von *Xenopus* Embryonen in einem standardisierten *in vivo* 24-Stunden-Testsystem quantitativ untersucht. Dabei werden die Haarzellen von behandelten Embryonen mit dem Fluoreszenzfarbstoff FM1-43FX angefärbt und die Fluoreszenzintensität mittels Fluoreszenzmikroskopie quantifiziert. Fünf zugelassene Gadolinium-enthaltende Kontrastmittel, Gadodiamid (Omniscan®), Gadobutrol (Gadovist®), Gadobenat dimeglumin (MultiHance®), Gadoterate meglumin (Dotarem®) und Gadopentetat dimeglumin (Magnograf® oder Magnevist®) wurden in Dosis-Wirkungsstudien eingesetzt um EC_{50} Werte (effektive Konzentrationen, welche die Färbung von Haarzellen um 50% reduzieren) zu ermitteln. Diese fünf Kontrastmittel repräsentieren alle vier Gruppen Gadolinium-basierter Kontrastmittel, basierend auf ihrer Konfiguration (linear oder makrozyklisch) und Ladung (ionisch oder nicht ionisch).

Für freies Gadolinium, welches als Ausganssubstanz diente, wurde ein EC_{50} Wert des Haarzellschädigungspotential von 9.7 µM ermittelt. Omniscan und Gadovist zeigten hingegen keine signifikante Haarzelltoxizität im gesamten getesteten Bereich von 1 bis 100 mM. Die anderen Kontrastmittel zeigten eine zunehmende Haarzell-Toxizität mit relative Fluoreszenzeinheiten von unter 75% bei Konzentrationen ab 50 mM. Auffällig war, dass MultiHance und Magnograf in Konzentrationen von 100 mM letal für *Xenopus* Embryonen waren. Deshalb wurden mögliche schädliche Wirkungen auf die Embryonalentwicklung von *Xenopus* detaillierter untersucht. Kontrastmittel-exponierte

Embryonen wurden über einen Zeitraum von fünf Tagen beobachtet. Freies Gadolinium war letal für 50 % der Embryonen in einer Konzentration (LC_{50}) von 56.7 µM. Ein Ansteigen der embryonalen Letalität wurde auch mit MultiHance, Magnograf und Dotarem beobachtet, doch waren die ermittelten LC_{50} Werte mit 50 und 110 mM massiv höher als die für Gadolinium. Eine Exposition mit Omniscan und Gadovist hatte hingegen keinen Einfluss auf die Embryonalentwicklung, selbst bei der Maximalkonzentration von 100 mM. Während die Ionizität ein wichtiges Merkmal für die Haarzell Toxizität und embryonale Letalität der Kontrastmittel war, war die Struktur des Liganden (makrozyklisch oder linear) weniger relevant.

Auf Basis der durchgeführten *Xenopus*-Experimente konnten folgende Schlussfolgerungen gemacht werden. Die Wichtigkeit der stabilen Bindung von Gadolinium zu seinem Chelat wurde unterstrichen durch die hohe Toxizität von freien Gadolinium für *Xenopus* Embryonen und die Haarzellen der Seitenlinienorgane. Die Haarzelltoxizitäten der geprüften Kontrastmittel war bei Konzentrationen, welche typischerweise bei intratympanalen Anwendungen zum Einsatz kommen, vernachlässigbar. Dies spricht dafür, dass diese Kontrastmittel sicher sind für den Einsatz bei der Innenohr-MRT. Die aktuellen Empfehlungen der European Medicines Agency (EMA) den Gebrauch der linear konfigurierten Kontrastmittel Omniscan, Magnograf und MultiHance auszusetzten, verdeutlichen die Wichtigkeit geringe Dosen, wie sie bei der intratympanal verstärkten Innenohr-MRT Methode zum Einsatz kommen, zu verwenden. Omniscan und Gadovist zeigten die besten Sicherheitsprofile unter den getesteten Kontrastmitteln. Die höhere Ablagerungsrate von Omniscan im menschlichen Körper favorisiert jedoch den Gebrauch von Gadovist für die intratympanale Applikation.

1 INTRODUCTION

Human beings perceive sound and keep balance with help of the inner ear. This vital sensory organ is located in a complex cavity in the temporal bone of the skull, known as the bony labyrinth. The inner ear is comprised of two functional compartments, the cochlea, required for hearing, and the vestibular system, dedicated to balance control. Specialized sensory cells, called hair cells, located in these two structures are responsible for transduction of motion and sound, respectively. Clinical conditions that interfere with inner ear function can cause temporary or chronic symptoms that may include hearing impairment, nausea, disorientation, vertigo, and dizziness. In Ménière's disease (MD), patients experience episodes of vertigo, tinnitus, and hearing loss. The cause of the disease is unclear and there is currently no cure. Magnetic resonance imaging using gadolinium-based contrast agents represents an important tool in the diagnosis of the MD. The gadolinium-based contrast agents (GBCAs) used in the procedure are considered to be safe, but certain aspects regarding their toxicity towards hair cells of the inner ear remain to be elucidated. The present study aims at addressing these issues using predictive *in vivo* tests with embryos and tadpoles of the African clawed frog, *Xenopus laevis*.

1.1 The Inner Ear

1.1.1 Anatomy

The human ear is divided into three compartments: the outer ear, the middle ear and the inner ear (Schuenke et al., 2010; Snow et al., 2009). The outer ear is the external portion of the ear consisting of the cartilaginous auricle and the external auditory canal. As shown in Fig. 1, the canal extends internally to the tympanic membrane, where it meets the middle ear. This structure consists of the air-filled tympanic cavity and includes the tree ossicles (malleus, incus, stapes), stabilizing ligaments, and the associated muscles. The Eustachian tube provides a connection between the middle ear and the upper throat.
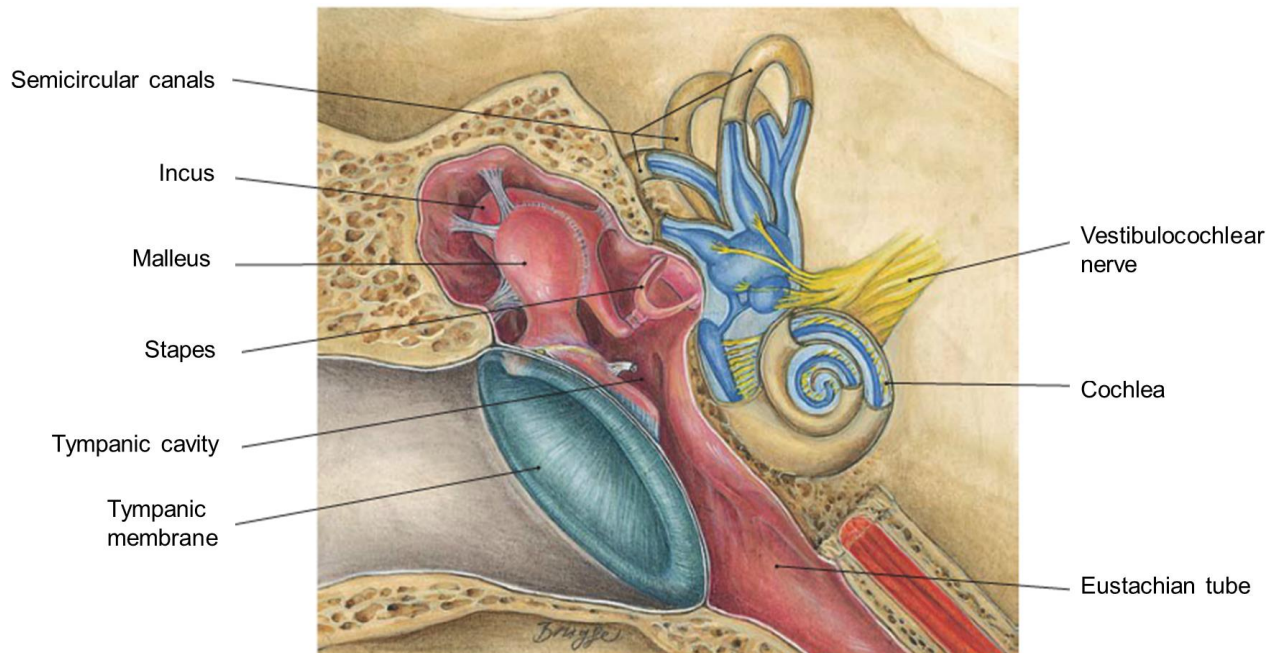
Fig. 1. Anatomy of the human middle and inner ear. Figure adapted from (Paulsen and Waschke, 2010).

The inner ear consists of the bony labyrinth, which is a system of ducts within the petrous part of the temporal bone, and the membranous labyrinth, a similar shaped tube system inside the bony labyrinth (Fig. 2). The space between them is filled with a fluid called perilymph and is connected to the subarachnoid space via the perilymphatic duct. By contrast, the membranous labyrinth is filled with endolymph and has a connection via the endolymphatic duct to the endolymphatic sac, an epidural pouch on the surface of the temporal bone. The endolymphatic duct widens into a membranous bulb, the endolymphatic sinus, and finally opens to the vestibule. The bony labyrinth has two membranous windows to the middle ear. The oval window separates the air-filled middle ear from the perilymph-filled inner ear and is the contact base to the chain of auditory ossicles (Schuenke et al., 2010). The membrane of the round window discloses three basic layers: an outer epithelium, a middle core of connective tissue, and an inner epithelium (Goycoolea and Lundman, 1997). The inner ear harbors the vestibular system and the cochlea, which are connected through the ductus reuniens (Goycoolea and Lundman, 1997; Schuenke et al., 2010).
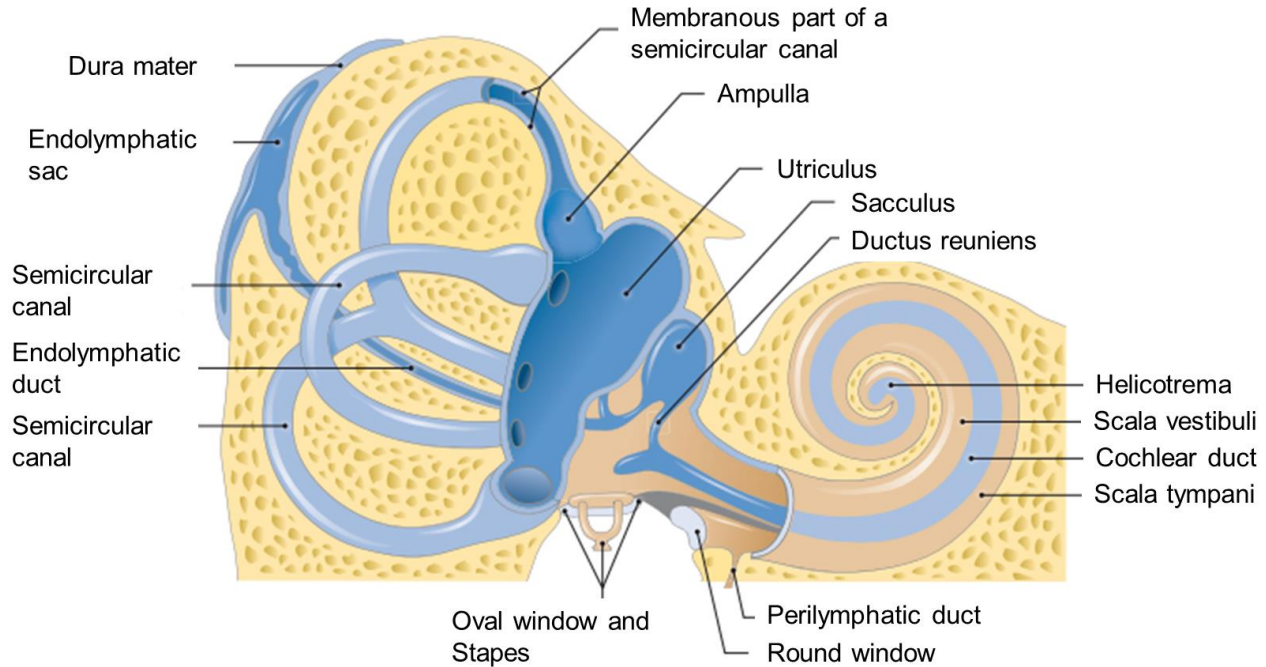
Fig. 2. Schematic drawing of the bony and membranous labyrinth comprising the inner ear. Figure adapted from (Tillmann, 2010).

1.1.1.1 The auditory apparatus

The cochlea is a spiral shell-shaped organ that is responsible for mediating auditory functions, i.e. the detection of sound waves. It is composed of three fluid-filled ducts or scalae (Fig. 3). The scala vestibuli and the scala tympani contain perilymph. The cochlear duct, also known as scala media, is filled with the endolymph and harbors the central sensory components. It is an extension of the membranous labyrinth and its circumference consists of three distinct membranes. The Reissner membrane defines the boundary to the scala vestibule. The outer wall of the cochlear duct is known as the spiral ligament. It serves as the basement for the stria vascularis, a multilayered organ composed of blood vessels and three distinct cell types. The marginal cells line the lumen of the scala media. The basal cells are found below the marginal cells, where the form a distinct epithelial layer. The intermediate cells are melanocyte-like and contain pigments. They are scattered throughout the stria vascularis. Finally, the basilar membrane forms the boundary between the cochlear duct and the scala tympani. It

serves as a template for the organ of Corti, which harbors the sensory cells of the auditory apparatus. The organ of Corti consists of hair cells and supporting cells. The hair cells are organized stereotypically into distinct rows. Three rows are occupied by the outer hair cells, while the inner hair cells are found in a single row. Hair cells are characterized by stereocilia emerging from the apical plasma membrane. They extend to the collagenous tectorial membrane and are interlinked by structures known as tip links (Schuenke et al., 2010; Schünke, 2011; Snow et al., 2009).
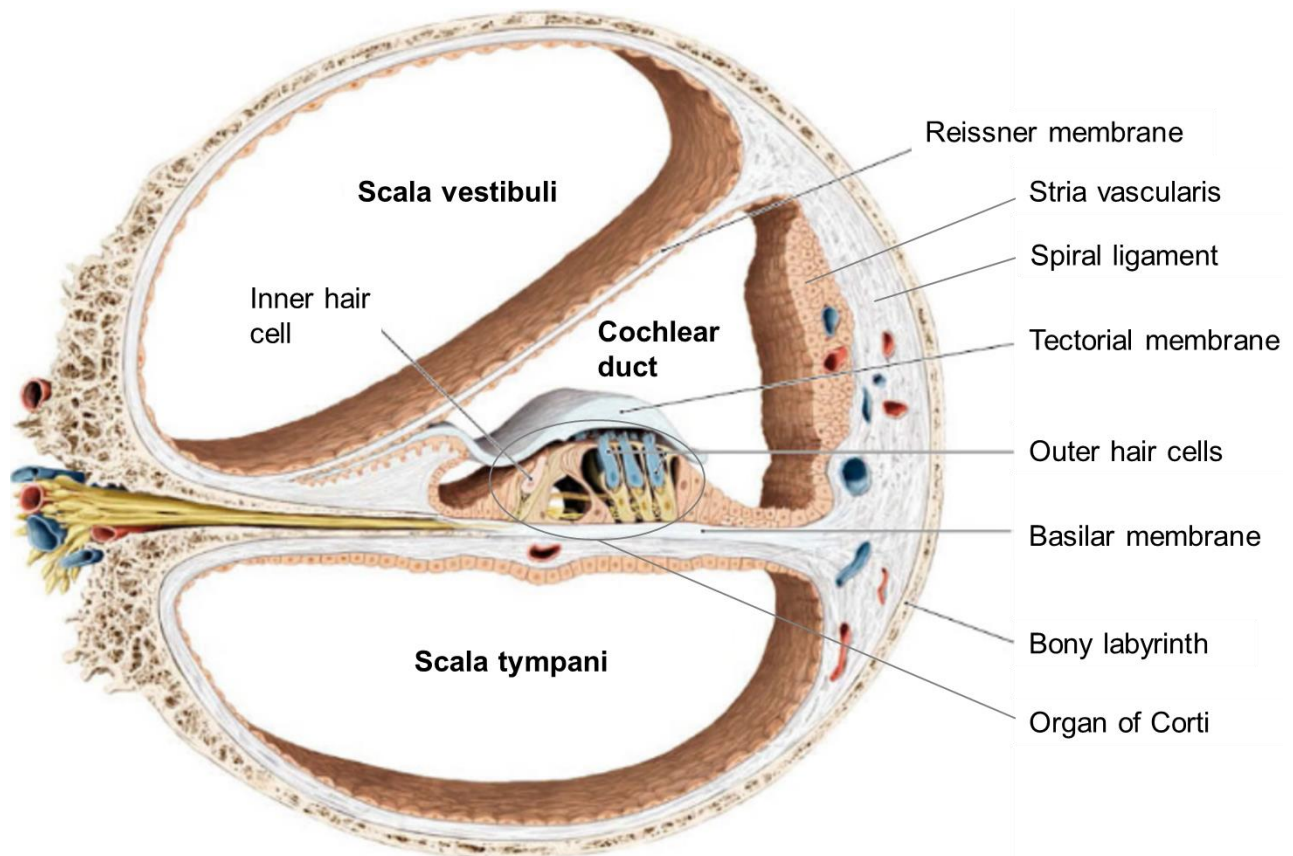
Fig. 3. Crossection of the cochlea illustrating the organ of Corti. The organ of Corti contains the sensory hair cells and is exposed to the endolymph of the scala media. Figure adapted from (Bley et al., 2015).

1.1.1.2 The vestibular apparatus

The vestibular labyrinth consists of three semicircular canals and the otolithic organs called saccule and utricle. The semicircular canals arise from the utricle and are coated by membraneous ducts. The semicircular ducts are organized orthogonally to each other

and they harbor ampullae, enlarged areas at one end that contain the sensory hair cells. As in the organ of Corti, the hair cells of the vestibular system bear apical stereocilia, but in addition they have one long kinocilium. The stereocilia are arranged in order of descending length with the kinocilium at one side (Schuenke et al., 2010). The hair cells of the ampullae are covered apically by a gelatinous mass, the cupula. The otolithic organs are located in the utricle and saccule. Their hair cells are similar to those of the ampullae. They are covered apically by a gelatinous extracellular matrix and a layer of calcium carbonate crystals, known as statoconia or otholith. Collectively this structure is known as the otolithic membrane. The lumen of all sections of the vestibular system is filled with endolymph (Purves et al., 2001).

1.1.2 Physiology

1.1.2.1 The auditory apparatus

The inner ear of vertebrates is the sensory organ which is able to perceive auditory and vestibular information. Pressure waves let the tympanic membrane, the chain of ossicles, and the oval window membrane vibrate. They reach the inner ear through transmission of this vibration to the perilymph, the basilar, and tectorial membrane. Since the basilar membrane is attached both, medially and laterally, and the tectorial membrane only at the spiral limbus, sound waves can deflect the stereocilia by shearing forces. Mechanoelectrical transduction (MET) channels located in the wall of the stereocilia and tethered to the tip links open or close due to the direction of deflection. Unselective cation currents from the endolymph into the hair cells, which are mainly borne by potassium and calcium ions, initiate the receptor potential that opens voltage gated calcium channels. The calcium ions trigger the basal release of neurotransmitters, which bind to the receptors of the corresponding neurons (Fig. 4). The action potentials induced in the afferent neurons of the acoustic nerves travel to the brainstem and terminate in the auditory cortex (Snow et al., 2009). The outer hair cells amplify the tectorial membrane movements by contraction and relaxation, also known as electromotility. This amplifying system is only present in mammals and increases the hearing sensitivity and sound frequency discrimination (Brownell et al., 1985). Finally, the round window bulges out when pressure in the labyrinth rises and it acts as a pressure valve (Fettiplace and Kim, 2014; Snow et al., 2009).
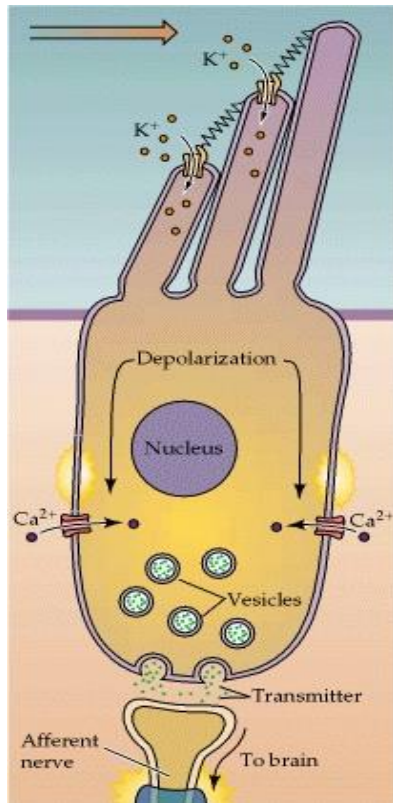
Fig. 4. Mechanoelectrical transduction in human cochlear hair cells. When the tectorial membrane shifts against the basilar membrane stereocilia deflect and the cation channels open. This leads to a calcium influx via voltage gated calcium channels and releases neurotransmitters which create the action potential in the neuron. Figure adapted from (Lewis and Hudspeth, 1983)

1.1.2.2 The vestibular apparatus

The vestibular system functions together with the proprioceptive and the visual systems in the sense of balance and spatial orientation. The semicircular ducts respond to angular acceleration, whereas the otolithic organs detect gravity and linear acceleration. During angular acceleration of the head, the inertia of the endolymph causes a shift in the cupula, which is detected by the hair cells of the sensory epithelium in the ampullae. The deflection of stereocilia alters the frequency of neurotransmitter release and the induction of action potentials in the afferent vestibular nerve that signals to the vestibular nucleus (Schünke, 2011; Snow et al., 2009). The vestibular hair cells are also responsible for the vestibulo-ocular reflex, which stabilizes images on the retina during head movements by producing compensatory eye movements (Schubert and Minor, 2004). By contrast, the kinocilia of hair cells located in the otolithic organs sense vertical and horizontal head acceleration by detecting inertia of the otoliths (Purves et al., 2001).

1.1.2.3 The cochlear fluids

The maintenance of homeostasis of the cochlear fluids is essential to create electric potential differences. The entire epithelium of the cochlear duct is sealed by intercellular tight junctions and thereby forms the cochlear "perilymph–endolymph barrier". While the composition of cochlear perilymph resembles that of the extracellular medium, the composition of cochlear endolymph is more similar to that of the cytosol (Table 1). With an electrode in the scala media a constant direct current of +80 mV, termed endocochlear potential, can be recorded at rest, see also Fig. 4 (Eckhard et al., 2014; Snow et al., 2009).

Table 1: Composition of cochlear and related fluids

	Cochlear Perilymph	Cochlear Endolymph	Cerebrospinal Fluid	Cytosol
Na^+, mM	148	1.3	149	12
K^+, mM	4.2	157	3	139
Cl^-, mM	119	132	129	4
HCO_3^-, mM	21	31	19	12
Ca^{2+}, mM	1.3	0.023		0.0002
Protein, mg/ml	178	38	24	100
pH	7.3	7.5	7.3	7.4

Table adapted from (Lang et al., 2007)

The cochlear perilymph has some similarities to the cerebrospinal fluid e.g. high Na^+ and low K^+ concentrations. As mentioned earlier the perilymph is continuous with the cerebrospinal fluid via the trabecular meshwork of the perilymphatic duct, but is believed to be produced partially by blood ultrafiltration in the stria vascularis (Kellerhals, 1976).

The K^+-rich and Na^+-poor endolymph is formed and maintained by the intermediate cells of the stria vascularis and by dark cells near the ampullae, both cells types are derived from of melanocyte precursors. The endolymph is likely to be absorbed in the endolymphatic sac, but there is also evidence suggesting that the endolymphatic sac is able to produce endolymph (Kimura, 1967; Rask-Andersen et al., 1999). The endolymphatic sinus may also play an important role in volume regulation, as it acts as a

mechanical valve to limit endolymph flow to the endolymphatic sac when there is a sustained positive pressure in the vestibule (Salt and Rask-Andersen, 2004). Overall, ion homeostasis of the different cochlear fluids is essential for the maintenance of the different physiological functions of the inner ear.

1.2 Meniere's Disease

Meniere´s disease (MD) is a disorder of the inner ear causing episodic attacks of vertigo, hearing loss and tinnitus. It has been defined as "the syndrome of endolymphatic hydrops" (Monsell et al., 1995). Its accurate diagnosis is difficult and complex. In addition, the underlying pathophysiology of the disease is poorly understood. Diagnosis and ethology of MD are therefore central issues in MD research.

1.2.1 History

The French physician Prosper Ménière described a series of patients with episodic vertigo and hearing loss in 1861. Together with the postmortem analysis of a young girl who suffered from vertigo after a hemorrhage into the inner ear, vertigo was no longer thought to be a cerebral symptom, but could also originate from a pathological process in the semicircular canals of the inner ear (Baloh, 2001; Lustig and Lalwani, 1997).

The Committee on Hearing and Equilibrium formed by the American Academy of Otolaryngology and the Head and Neck Surgery Foundation (AAO-HNS CHE) defined MD as "recurrent, spontaneous episodic vertigo; hearing loss; aural fullness; and tinnitus. Either tinnitus or aural fullness (or both) must be present on the affected side to make the diagnosis." As there is still no final agreement on the pathophysiology, the AAO-HNS Committee further stated: "For reporting purposes, Meniere's disease is a clinical disorder defined as the idiopathic syndrome of endolymphatic hydrops." (Monsell et al., 1995).

1.2.2 Current diagnostic criteria for MD

In August 2015 a consensus document of the AAO-HNS, the Japanese Society for Equilibrium Research, the European Academy of Otology and Neurotology, Bárány Society, and the Korean Balance Society stating the diagnostic criteria for MD was

published. It contains revised diagnostic criteria and distinguishes between possible, probable, definite and certain MD (Lopez-Escamez et al., 2015).

(i) Possible MD

Every episodic vertigo or fluctuating hearing loss can be considered as possible MD.

(ii) Probable MD

Each of the following three criteria are used to indicate probable MD:

A. Two or more episodes of vertigo or dizziness, each lasting 20 minutes to 24 hours

B. Fluctuating aural symptoms (hearing, tinnitus or fullness) in the affected ear

C. Not better accounted for by another vestibular diagnosis

(iii) Definite MD

The follow criteria have to be met:

A. Two or more spontaneous episodes of vertigo, each lasting 20 minutes to 12 hours

B. Audiometrically documented low- to medium- frequency sensorineural hearing loss in the affected ear on at least one occasion before, during or after one of the episodes of vertigo

C. Fluctuating aural symptoms (hearing, tinnitus or fullness) in the affected ear

D. Not better accounted for by another vestibular diagnosis

(iv) Certain MD

The diagnosis requires all criteria for definite MD plus a postmortem histopathological confirmation of endolymphatic hydrops.

However, there have been several attempts at defining simple clinical diagnostic criteria in the past (Gurkov and Hornibrook, 2018). Each of them has its limitations, including the most recent proposal by the Barany Society (Lopez-Escamez et al., 2015). As a consequence of the evidence gathered by the morphologic clinical *in vivo* diagnosis of

endolymphatic hydrops, a new terminology has been developed: Hydropic Ear Disease (Gurkov et al., 2016).

1.2.3 Differential Diagnosis

There are several differential diagnoses to be considered and excluded in the diagnosis of MD. These assessments require extensive and time-consuming evaluations, which may be perceived as unpleasant by patients. The assessments may include audiometry, vestibular evoked myogenic potentials testing, rotatory chair testing, dehydration tests, electrocochleography, and video head impulse test. In addition, MRI of the head with an intravenous applied contrast agent may be required to exclude oncogenic causes, such vestibular schwannoma or endolymphatic sac tumor (Lopez-Escamez et al., 2015; Plontke and Gurkov, 2015).

The differential diagnoses of MD include transient ischemic attack or stroke, since an interruption of the blood supply from the vertebro-basilar circulation to the inner ear can cause combined audio-vestibular symptoms (Oas and Baloh, 1992), and vestibular migraine. The latter manifests with features overlapping with MD, not only in symptoms, but also in the histopathology, given that endolymphatic hydrops can be found in many cases (Gurkov et al., 2014). Migraine and benign paroxysmal positional vertigo do not explain the complete spectrum of MD symptoms and should be considered as co-morbidities (Lopez-Escamez et al., 2015). Other conditions include monogenetic hereditary disease of sensorial hearing loss and further examples listed in Table 2. Psychogenic vertigo is also an important differential diagnosis, although it is not mentioned in this list.

Table 2. Differential diagnosis of Meniere's disease

Autosomal dominant sensorineural hearing loss type 9
Autosomal dominant sensorineural hearing loss type 6/14
Autoimmune inner ear disease
Cerebrovascular disease (stroke/TIA in the vertebrobasiliar system/bleeding)
Cogan's syndrome. Some cases may have recurrences.
Endolymphatic sac tumor
Meningiomas and other masses of the cerebellopontine angle
Neuroborreliosis

Otosyphilis

Susac syndrome

Third window syndromes (Perilymph fistula, canal dehiscence, enlarged vestibular aqueduct)

Vestibular migraine

Vestibular paroxysmia (neurovascular compression syndrome)

Vestibular schwannoma

Vogt-Koyanagi-Harada syndrome

Table adapted from (Lopez-Escamez et al., 2015)

1.2.4 Epidemiology

MD is with a prevalence of about 190-513 per 100.000 one of the most common inner ear disorders. It is more common in older female patients of Caucasian background, (Alexander and Harris, 2010; Havia et al., 2005; Tyrrell et al., 2014).

In Caucasian patients, evidence for familial MD is observed in 8-9% of the cases examined. Genetic heterogeneity with autosomal dominant inheritance is suspected, but clinical differences are currently not obvious (Requena et al., 2014).

1.2.5 Pathophysiology

The central and pathognomonic pathology of MD is endolymphatic hydrops (ELH). Nevertheless, the etiology of ELH is largely unknown, as are the exact pathophysiologic consequences of ELH. Today it is known, that ELH can arise spontaneously (Primary Hydropic Ear Disease) or as a consequence of a wide range of serious lesions of the inner ear (Secondary Hydropic Ear Disease). The spontaneous remission of rotatory vertigo attacks in MD is observed in over 50% of the affected patients within 2 years and in over 70% after 8 years. However, many patients are left with poor balance control and impaired hearing (Minor et al., 2004).

ELH is thought to result from the accumulation of the endolymph and alterations of its composition in the endolymphatic duct and the vestibular organs. This causes the Reissner membrane bulge out and the endolymphatic space is distended into the scala vestibuli, affecting mostly the cochlea and sacculus. These effects may also extend to the utricle and semicircular canals (Kimura, 1967; Merchant et al., 1995). The degree of displacement of the boundary membranes of the endolymphatic space is highest in the apex of the cochlea. As a consequence, sound perception is impaired particularly in low

to medium frequency range (see also 1.2.2). Rupture of the membranes may cause acute vertigo, tinnitus, and hearing loss attacks, probably by causing electrolyte intermixture (Salt and Plontke, 2010). In humans, the ELH can occur idiopathic or be caused by specific disorders e.g. infectious labyrinthitis, noise induced hearing loss, or vestibular schwannoma (Plontke and Gurkov, 2015).

The development of an ELH in MD is thought to be caused by either by (i) a decrease in endolymph drainage, or (ii) an increase in endolymph production.

As mentioned earlier, the endolymphatic sinus is believed to act as one-way valve. It either allows the flow of the endolymph to the endolymphatic sac or prevents it. Hence, dysregulation could lead to hydrops formation (Salt and Rask-Andersen, 2004). In addition, destruction or any occlusion of the endolymphatic sac can cause accumulation of the endolymph (Kimura, 1967). Finally, the endolymphatic sac function can be altered by medication. For example, systemic catecholamines will cause an increase of the endolymphatic pressure (Inamoto et al., 2009).

With regard to mechanisms influencing endolymph production, changes in the ion composition of the endolymph can become osmotically relevant and induce volume expansion. Furthermore, longitudinal endolymph flows mediated by water permeation between the endolymph and perilymph via aqueous pores could contribute to ELH formation (Eckhard et al., 2014).

Importantly, postmortem histopathological analysis of the inner ear of patients diagnosed with definite MD has demonstrated the presence of ELH in nearly all cases studied. At present, the thesis that MD causes the development of ELH or that it is an epiphenomenon cannot be supported. The ELH appears to be necessary but not sufficient for MD manifestation. Vascular risk factors should be considered as possible cofactors (Foster and Breeze, 2013; Rauch et al., 1989). In summary, it is clear that further research in needed to clarify these issues. The recent development of MR imaging of the endolymphatic and perilymphatic space may contributed to novel insights and a better understanding of the pathophysiology of MD, as discussed in section 1.5.

1.3 *Xenopus,* a Versatile Vertebrate Model Organism for Biomedical Research

The clawed frogs of the *Xenopus* genus are aquatic frogs and belong to the Pipidae family of amphibians. The model organism *Xenopus* includes the species *Xenopus laevis* and *Xenopus tropicalis*, whose genomes are fully sequenced (Session et al. 2016). *Xenopus laevis* has been widely used for genetic, embryonic, and electrophysiological research, as well as for a historic pregnancy test (Hobson, 1958; James-Zorn et al., 2018; Sater and Moody, 2017). More recently, its value in drug discovery and development including drug target identification, lead compound discovery, and assessment of drug toxicity has been recognized (Wheeler and Brandli, 2009). As an amphibian, *Xenopus* frogs are evolutionary closer related to humans than for example fish. The latter have diverged about 455 million years ago from vertebrate evolution leading to modern-day mammals, while amphibians have done so an estimated 360 million years ago (Schmitt et al., 2014).

Since *Xenopus* frogs are obligatory aquatic, they can be easily housed in aquaria and do not require terraria. Minced meat or food pellets are sufficient for feeding the adults (Schmitt et al., 2014). Female frogs lay hundreds of eggs at one time, which can be fertilized *in vitro* permitting the generation of many embryos undergoing synchronous development (Wallingford et al., 2010). The embryos become transparent as development proceeds. The tadpole are robust in handling, develop fast, and show many morphological similarities the mammalian counterparts (Fig. 5). The skin is permeable to small organic molecules, which has been beneficial for drug screening and testing (Schmitt et al., 2014; Wallingford et al., 2010).
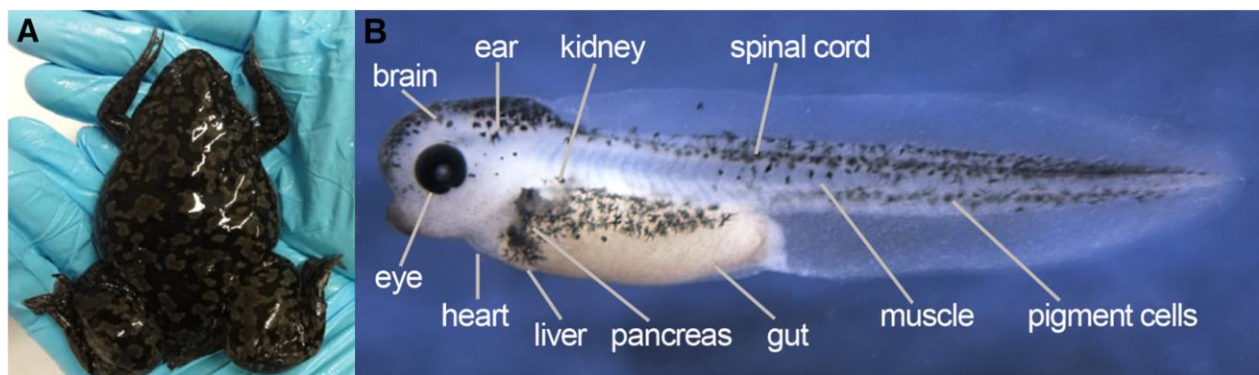
Fig. 5. The *Xenopus* animal model*.* A: Adult female *Xenopus laevis* frog. **B**: *Xenopus laevis* embryo at stage 41. Important organs of vertebrate organisms are indicated. Figures adapted from (Schmitt et al., 2014).

1.3.1 Anatomy and Development

The development of *Xenopus laevis* was systematically surveyed and described by Nieuwkoop and Faber in 1956. They defined 66 developmental stages from oocyte to the end of metamorphosis according to external and internal morphological criteria (Nieuwkoop and Faber, 1967). The fertilized egg (stage 1) of the poikilothermic *Xenopus laevis* frog develops temperature-dependent (Fig. 6). At 23 °C, the first cleavage division can be observed after 90 min (stage 2). The next eleven cleavages occur every 30 min. Yolk platelets are early consumed and the embryo becomes transparent quickly. Gastrulation, neurulation and the onset of the organogenesis continue to happen within 48-72 hours. The key organs of vertebrate body are established during the organogenesis period. This includes the cardiovascular system, the lymphatic vasculature, the digestive tract, excretory organs, the hematopoietic system, the central nervous system, eyes, the olfactory system, the inner ear with cochlear and vestibular organs, and the lateral line system (Fig. 5). Eight to twelve weeks after fertilization, metamorphosis sets in to transform the tadpole to an adult frog, which includes the development of limps and lungs. Unlike most other frog species, *Xenopus* remains full aquatic throughout adult life (Schmitt et al., 2014). Given the anatomical and histological similarities, hair cells of the lateral line can be used to assess the toxicity of substance that may be ototoxic (see 1.5. for details).
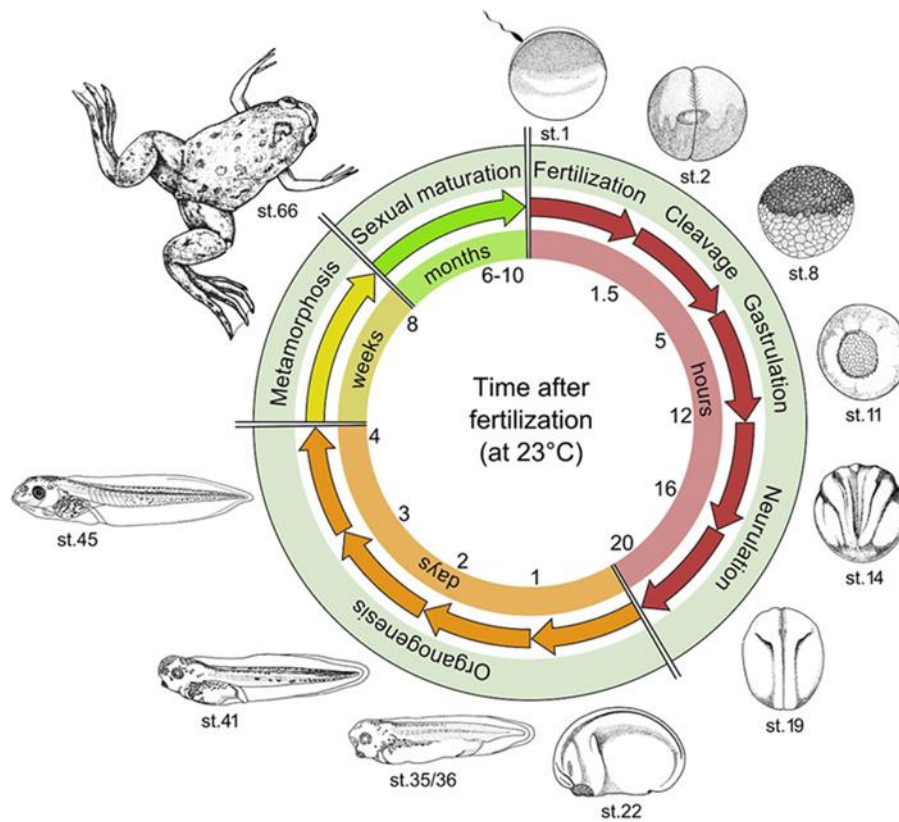
Fig. 6. The life cycle of _Xenopus laevis._ Major steps in development of _Xenopus_ individuals are illustrated. The time specifications refer to development at 23°C. Adapted from (Schmitt et al., 2014).

1.3.1.1 The lateral line system

The lateral line system is a sensory organ found in larval stages of fish and amphibians, and persist into adulthood in fish and aquatic amphibian. It is located in the epidermis of the body, where it functions in the detection of water flow. Therefore, it plays an imported role in feeding, swimming, navigation and communication behaviors (Coombs et al., 2013). In amphibians, cranial ectodermal sensory placodes migrate during embryogenesis along the head and trunk to form characteristic lines of differentiating, superficial neuromasts (Fig. 7). Each organ consist of a functional unit comprised of mechanosensitive hair cells, which share many morphological and functional similarities with the hair cells of the mammalian inner ear. Hair cells of the lateral line and the inner ear are probably derived from an evolutionary related sensory placode (Baker, 2008; Kalmijn, 1989). The hair cells extend into one kinocillium and a bundle of linked stereocilia. They are embedded in a gelatinous cupula, which is secreted by supporting cells (Baker, 2008). Water flow induced drag forces deflect the cilia. This creates an electric potential that travels via the afferent fibers to the hindbrain. The efferent innervation suppresses self-stimulation from self-movements and -vocalization (Baker, 2008).
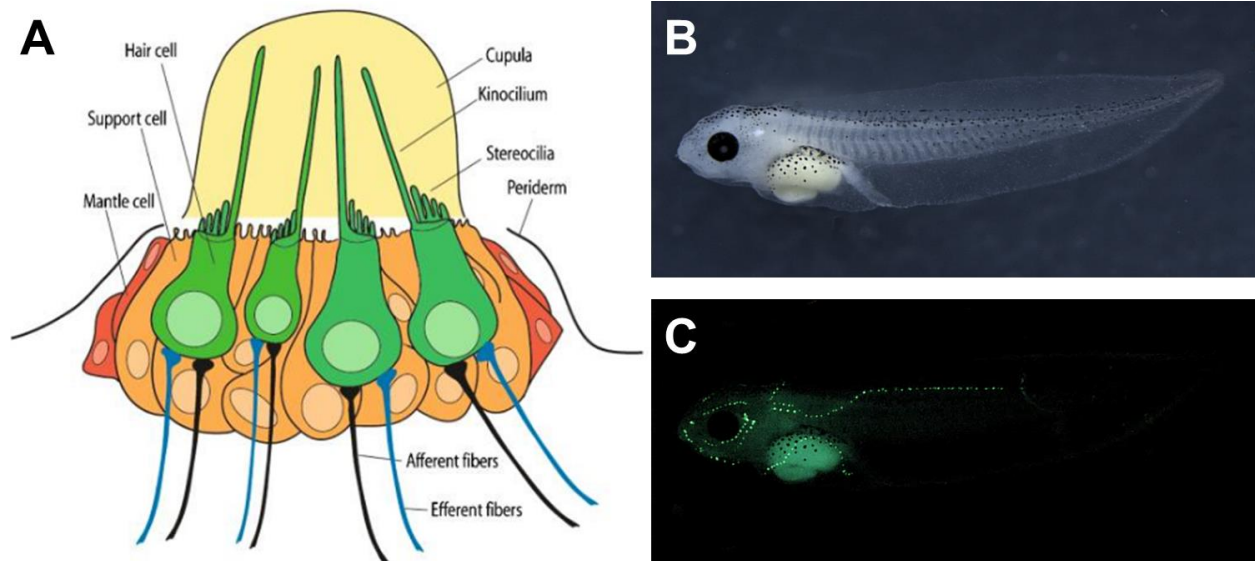
Fig. 7. The lateral line system. A: Schematic illustration of superficial neuromast of the lateral line. Each neuromast of the lateral line contains several hair cells, support and mantle cells. The green illustrated hair cells cilia are embedded in the gelatinous cupula. Figure adapted from (Chiu et al., 2008). **B**: *Xenopus* embryo at stage 45 (bright field image). **C**: Fluorescence image of the same embryo displaying fluorescently stained lateral line organs. The staining in developing gut is results from auto-fluorescing yolk platelets.

1.4 Gadolinium-based Contrast Agents

1.4.1 Gadolinium

Gadolinium is a naturally occurring chemical element with the atomic number 64. It is rare-earth heavy metals of the lanthanide group with strong paramagnetic properties. Its trivalent ions, gadolinium (III) (Gd^{3+}), have seven unpaired electron spins, which are responsible for its enormous paramagnetic properties above 20°C with strong relaxation effects. Given these unique physical properties, gadolinium has become a major constituent of contrast agents for MRI. Free Gd^{3+} is however highly toxic as it has a similar ionic radius compared with Ca^{2+}. As demonstrated in animal studies, Gd^{3+} competes with Ca^{2+} ions and, as a trivalent ion, it binds with higher affinity to target proteins (Sherry et al., 2009). The median lethal dose (LD_{50}) for intravenously administered Gadolinium in rats has been estimated at 0.5 mmol/kg (Gries, 2002). To

avoid the toxicity of free Gd^{3+}, the cation is always chelated with polyaminopolycarboxylic acids that serve as ligands. In addition, chelation also preserves the paramagnetic properties of Gd^{3+}. Nevertheless, Gd^{3+} can also be set free despite chelation. For example, endogenous anions may have higher affinity for gadolinium ions than the ligand. Alternatively, endogenous cations may compete with gadolinium for binding to the ligand (Ramalho et al., 2016). This exchange process is known as transmetallation (Haley, 1965; Hirano and Suzuki, 1996; Sherry et al., 2009). Possible toxic effects of free gadolinium ions include the induction of apoptosis, the release of chemokines, and increased oxidative stress (Rogosnitzky and Branch, 2016).

Importantly, gadolinium ions are able to block various mechanically gated channels, such as baroreceptors that sense pressure changes in rats (Kraske et al., 1998). Yang and Sachs used *Xenopus* oocytes expressing stretch-activated channels to study the effects of gadolinium (Yang and Sachs, 1989). They found a concentration-dependent block of channel opening after gadolinium treatment.

At a gadolinium concentration of 5 µM the probability of a channel being open was about 10^{-1}, whereas at 10 µM the value dropped to less than 10^{-5} (Yang and Sachs, 1989). Studies across different model organisms provide compelling evidence that gadolinium ions have toxic effects on hair cells of the inner ear by interfering with MET channel functions. Cochlear hair cells of chicken, turtles, and guinea pigs were found to be susceptible to gadolinium-induced toxicity resulting in the blocking of MET currents (Farris et al., 2004; Kimitsuki et al., 1996; Santos-Sacchi, 1991). Expression of the transient receptor potential channel vanilloid subfamily member 4 (TRPV4) is associated with inner and outer hair cells, supporting cells, and marginal cells of the inner ear (Takumida et al., 2005). Since gadolinium can block TRPV4 functions (Andrade Yé et al., 2005), TRPV4 might mediate some of the toxic effects of free gadolinium ions on hair cells of the inner ear. As outlined below, the toxic effects of free gadolinium extend beyond the inner ear (see 1.4.2.2.). Taken together, the safe application of gadolinium in contrast agent for MRI requires its stable ligation to a carrier molecule in order to minimize the toxic effects of free gadolinium ions.

1.4.2 Gadolinium-based Contrast Agents for MRI

Several metal ion chelates were developed over the last 30 years to overcome the toxicity of free gadolinium ions (Runge et al., 2011). These chelates differ in their biodistribution, which is useful for specific applications of GBCAs. When injected intravenously, GBCAs rapidly equilibrate in the intravascular and extracellular compartment. The biological elimination half-life is about 1.5 - 2.0 hours in patients with normal renal function (Bellin and Van Der Molen, 2008). GBCA indications include the contrast imaging of vessels by MR angiography or the imaging of pathological processes in the central nervous system, mainly tumors, with GBCAs that penetrate the blood-brain barrier (Runge et al., 2011). The five GBCAs that were examined in the present study are classified as extracellular fluid agents or intravenous contrast agents. They are approved for human applications by the European Medicines Agency (EMA) and the U.S. Food and Drug Administration (FDA). Their chemical structures are shown in Fig. 8. They represent examples of the major subclasses of GBCAs. In the context of the present work, brand names will be used in place of the compound names (see Table 3) enabling the reader to better distinguish the different GBCAs.
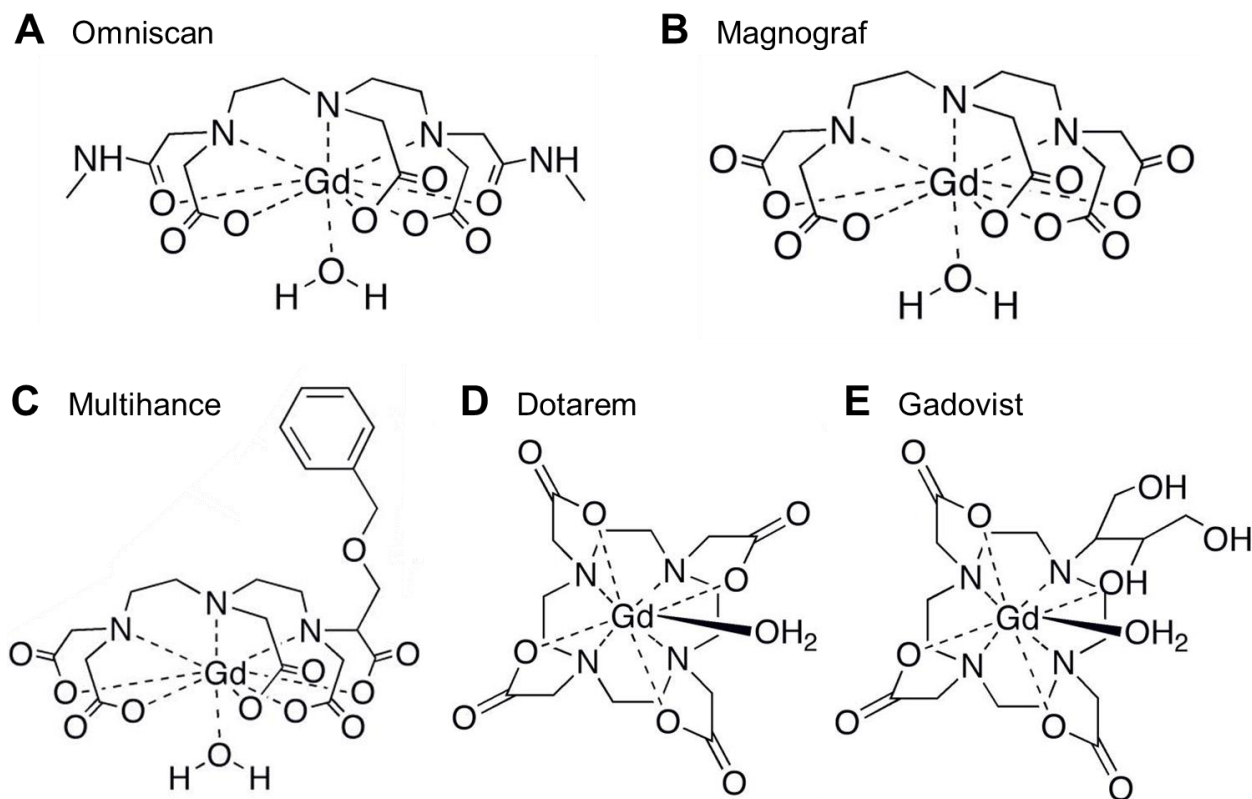
Fig. 8. Chemical structures of selected GBCAs. All GBCAs depicted consist of ligands that enable 8-coordinate binding to gadolinium. In each case, there is a single water molecule bound to gadolinium. The GBCAs shown are examples of non-ionic (A) and ionic linear ligands (B, C) as well as ionic (D) and non-ionic macrocyclic ligands. Figure adapted from (Aime and Caravan, 2009).

1.4.2.1 Classification and chemical properties of GBCAs

There are four different classes of GBCAs based on the type of the ligand structure (macrocyclic or linear) and its charge (ionic or non-ionic) (Idée et al., 2014; Sherry et al., 2009). Macrocyclic ligands fully capture the gadolinium ion in a preorganized cubic cavity, whereas linear ligands bind the ion using an open-chain structure. Regarding ionic GBCAs, they harbor counterions bound via ionic bonds to the ligand that dissociate in water and increase the osmolality. The presence of counterions can contribute to the toxicity of GBCAs (Kun and Jakubowski, 2012). The differences in the chemical structures impact the kinetic and thermodynamic stability of GBCAs. In an assessment of complex stability under conditions similar to those in the human body, ionic macrocyclic GBCAs showed the highest stability, followed by the ionic linear ones,

whereas the nonionic linear chelates released gadolinium the most (Frenzel et al., 2008) (Sherry et al. 2009). Key physiochemical characteristics of the five GBCAs studied in the present work are summarized in Table 3. All five GBCAs are eliminated by renal filtration, except from MultiHance. The latter contains a benzyl group (Fig. 8) enabling hepatic uptake and clearance (Aime and Caravan, 2009). The recommended standard dosing of GBCAs is 0.1 mmol/kg, but this may change depending on the specific indication and vary from country to country (Aime and Caravan, 2009; Runge et al., 2011). The equilibrium process of dissociation of gadolinium and the chelate can be measured by applying heat. The thermodynamic constant is determined at pH 1, whereas the conditional stability constant is measured at pH of 7.4, which is more appropriate when considering the *in vivo* situation, The higher these constants are, the more energy is needed to release gadolinium from the chelate (Ramalho et al., 2016). Kinetic stability represents an alternative approach to assess GBCA stability. It refers to the dissociation half-life at pH 1 and 25°C (Port et al., 2008). The solubility of an organic compound in aqueous solutions is determined by its hydrophilicity. One measure of hydrophilicity is the logP value, which is defined as the ratio of the concentrations of the test compound in a mixture of two immiscible phases (octanol and water) at equilibrium. Hydrophilic substances carry negative logP values.

Table 3. Characteristics of GBCAs

Brand Name	Omniscan	Magnograf	MultiHance	Dotarem	Gadovist
Generic Name	Gadodiamide	Gadopentetate-dimeglumine	Gadobenate-dimeglumine	Gadoterate-meglumine	Gadobutrol
Acronym	Gd-DTPA-BMA	Gd-DTPA	Gd-BOPTA	Gd-DOTA	Gd-DO3A-Butrol
Manufacturer	GEHealthcare	Bayer	Bracco	Guerbet	Bayer
Ligand Type	Linear	Linear	Linear	Macrocyclic	Macrocyclic
Ionicity	Non-ionic	Ionic	Ionic	Ionic	Non-ionic
Clearence	Renal	Renal	Renal (96%) Hepatic (4%)	Renal	Renal
Dosing (mmol/kg)	0.1	0.1	0.05 - 0.1	0.1 - 0.2	0.1
Osmolarity (Osm/kg H_2O, 37°C)	0.79	1.96	1.97	1.37	1.60
$logK_{therm}$	16.9	22.1	22.6	25.6	21.8
$logK_{cond}$	14.9	17.7	18.4	19.3	14.7
$T_{1/2}$	> 5 sec	> 5 sec	> 5 sec	338 hours	43 hours
logP (octanol:water)	- 2.13	- 3.16	- 2.33	- 2.87	- 2.0
Molecular mass (g/mol)	592	938	1058	754	605

Abbreviations: K_{therm}, thermodynamic stability constant; $K_{cond.}$, conditional stability constant; $T_{1/2}$, dissociation half-time at pH 1.0 and 25°C. Table contains data taken from published sources (Runge et al., 2011) (Idée et al., 2014) (Bennett et al., 2012).

1.5 Magnetic Resonance Imaging of the Inner Ear

In the past decade, advances in MRI of the inner ear, particularly the ability to discriminate between the perilymphatic and endolymphatic spaces, have been key for the diagnosis and the characterization of the pathology of diseases associated with ELH. The importance of MRI for the differential diagnosis of MD and vestibular migraine has been reviewed recently (Gurkov et al., 2014). The key findings regarding MD's pathophysiology obtained by MRI include that (i) the cochlear and vestibular labyrinths can be differently affected; (ii) the degree of ELH correlates with duration and degree of symptoms, and (iii) the clinically asymptomatic contralateral ear often contains also an ELH, suggesting MD is a systemic disease (Gurkov et al., 2016; Plontke and Gurkov, 2015; Pyykko et al., 2013). Visualization of ELH by MRI can be performed by two distinct approaches that rely on applying the GBCAs either (a) intratympanically or (b) intravenously as detailed below.

1.5.1 Intratympanic Enhanced Inner Ear MRI

The first successful visualization of ELH in humans was achieved by three-dimensional fluid attenuated inversion recovery (3D-FLAIR) MRI at 3 Tesla (3T) after intratympanic application of gadolinium hydrate (Nakashima et al., 2007). The method was subsequently improved by employing the 3D inversion-recovery turbo spin echo (3D-IR TSE) sequence (Naganawa et al., 2008). This modification permitted not only the imaging of the endolymphatic and the perilymphatic space, but also the surrounding bone structures could be visualized (Fig. 9).
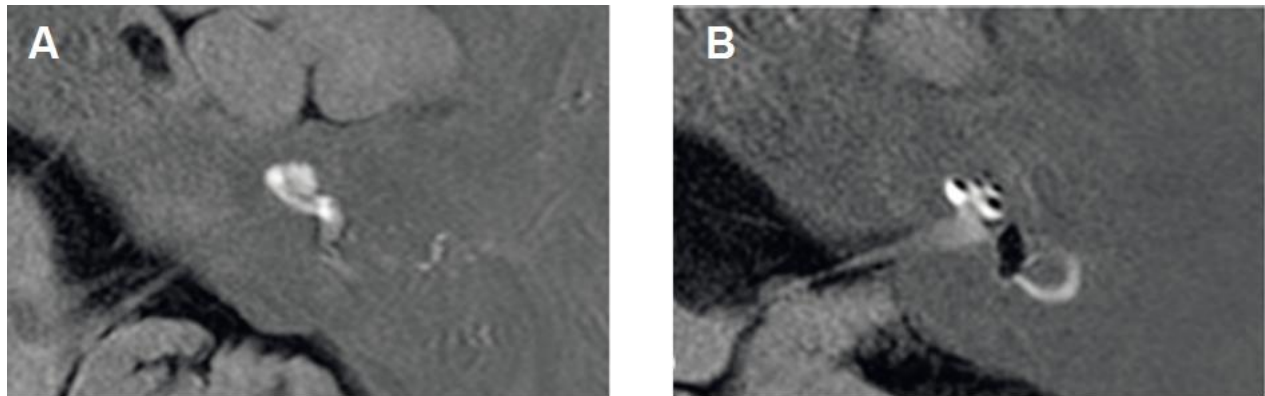
Fig. 9. Axial 3D-IR TSE MRI of the left inner ear. A: Healthy left inner ear, no evidence for EH; **B**: marked EH, the hypointense areas correlate with the enlarged, out bulging endolymphatic space. Figure adapted from (Gurkov et al., 2012).

After intratympanic application of GBCAs, the agent appears to selectively enter the perilymphatic compartment by diffusion mainly via the oval, but also via the round window (Zou et al., 2012). However, GBCA uptake into the inner ear has been reported to be insufficient in five to ten percent of the treated patients (Gurkov et al., 2016). Intratympanic enhanced MRI was also found to be helpful in predicting the ability of intratympanically injected drugs, such as steroids and gentamicin used to treat MD, to diffuse in the inner ear (Yamazaki et al., 2012). It should be emphasized that the intratympanic use of GBCAs is currently still off-label.

1.5.1.1 Intratympanic GBCA-enhanced inner ear MRI

Standardized approaches for intratympanic GBCA injection followed by MRI are currently in development. An example of a currently used protocol is described next. 20 - 28 hours before MRI, the external auditory canal is cleaned. The procedure is initiated anesthetizing the tympanic membrane with 4% tetracaine. Subsequently, the 0.5 mM GBCA stock is diluted eightfold with physiological saline to a final concentration of 62.5 mM. 0.4 ml of the diluted GBCA solution is injected under microscopic control into the middle ear. After the injection, the patient will be put into the supine position (lying horizontally with the face and torso facing up). The head will be turned 45° to the opposite side for 30 min without speaking or swallowing to allow the GBCA to diffuse into the inner ear prior to MRI (Bykowski et al., 2015; Gurkov et al., 2016). Various combinations of scanners and coil models/channels have been utilized for the detection of ELH by GBCA-enhanced MRI. A field strength of 3 Tesla is generally required

(Gurkov et al., 2016). To date, the best image quality is achieved using a hybrid of 16-ch head coil and ear coil (loop 7 cm) (Zou J, 2015). Furthermore, computer-aided segmentation of endo- and perilymphatic spaces was developed to evaluate the obtained MR images in a quantitative and observer-independent manner (Zou J, 2015).

1.5.2 Intravenous GBCA-enhanced Inner Ear MRI

Intravenous injection of GBCAs represents an alternative method for inner ear MR that permits the discrimination between the perilymphatic and endolymphatic spaces. This second method relies on the observation that the blood-perilymph barrier is not as tight and impenetrable as the blood-endolymph barrier (Zou et al., 2009). For many years, the required intravenous doses of GBCAs that would enable sufficient GBCA delivery to the perilymph were considered too high and not tolerable. For this reason, the intratympanic GBCA application was initially favored and investigated in detail. In 2010, however, the first successful visualization of ELH after intravenous administered GBCAs was reported (Nakashima et al., 2010). Specifically, a doubling of the GBCA dose to 0.2 mmol/kg was required and the perilymph signal intensity was lower compared to intratympanic GBCA applications. Subsequently, further improvements in MRI technology allowed for a 50% reduction of the GBCA dose (Naganawa et al., 2012). Specifically, the improved protocol uses a standard dose of GBCA (Omniscan, 0.1 mmol/kg), which is injected intravenously four hours prior to MRI. A 3T MR subtraction technique, known HYDROPS2 (hybrid of reversed image of MR cisternography and positive perilymph signal by heavily T2- weighted 3D-FLAIR) was employed to visualize ELH (Naganawa et al., 2012).

1.5.3 Comparison between Intratympanic and Intravenous GBCA-enhanced Inner Ear MRI

The advantages and disadvantages of the two GBCA-enhanced inner ear MRI methods are summarized in Table 3. Importantly, systemic adverse side effects are more likely to occur after intravenous than intratympanic GBCA administration given the much higher dose of GBCA required, 7 mmol vs. 0.025 mmol, respectively (see below for details). Irrespective of the administration method used, GBCAs may reach the hair cells in the endolymphatic compartment raising the possibility of GBCA-induced ototoxicity. To date, this notion could however not been corroborated in experimental studies using guinea

pigs or mice (Counter et al., 2000) (Counter et al., 2013). For example, high resolution images of strong field (9.4 T) MRI in mice could not detect a GBCA-increased signal intensity in the endolymph, when applied intravenously (Counter et al., 2013). Furthermore, a comparison of the two GBCA application methods by inner ear MRI in mice revealed no differences in GBCA permeation into endolymph (Zou et al., 2010). More recently, first studies using a combination of an intravenous and intratympanic GBCA injections have provided promising results warranting more detailed investigation (Iida et al., 2013; Naganawa et al., 2014). According to our clinical experience, intratympanic contrast application has a greater ability to detect mild ELH than intravenous contrast application, due to its stronger signal-to-noise ratio (Plontke and Gurkov, 2015). It should further be kept in mind that the total dose in the intratympanic route is about 500-fold lower than in the intravenous route.

Table 3. Comparison of intratympanic and intravenous GBCA-enhanced inner ear MRI

	Intratympanic Method	Intravenous Method	References
Signal intensity in perilymph	Higher	Lower	(Nakashima et al., 2010; Yamazaki et al., 2012)
Total GBCA dose	Lower (~ 0.025 mmol)	Higher (~ 7 mmol)	(Gurkov et al., 2016)
Average success rate (Causes of failure)	90% - 95% (insufficient GBCA uptake into perilymph)	95% (claustrophobia, gross motion, metal artifact)	(Gurkov et al., 2016; Naganawa and Nakashima, 2014)
Waiting time	24 hours	4 hours	(Gurkov et al., 2016; Naganawa et al., 2012)
Potential ASE	Primarily local	Systemic	

1.6 Toxicity of GBCAs

GBCAs used at the recommended doses for MRI were initially considered to be relatively nontoxic for the human body. In the last decade, however, reports about severe adverse effects, mostly in patients with reduced renal function, have begun to emerge. In patients with renal insufficiency, renal elimination of GBCAs is reduced, gadolinium ions dissociate from the chelate, and they accumulate in the body, where they initiate a specific type of fibrosis, termed nephrogenic systemic fibrosis (NSF). The symptoms of NSF range from erythema, subcutaneous nodules in the skin, over painful muscle and joint contractions with reduced mobility to fibrosis of inner organs like lung, heart, and liver. The diagnosis is mostly made by taking a skin biopsy. The prognosis is at present unfavorable as there are still no effective treatment options (Cheong and Muthupillai, 2010; Grobner, 2006; Rogosnitzky and Branch, 2016). The estimated incidence of NSF (for the period from 2003 to 2006) is at 36.5 cases per 100'000 GBCA administrations (Perez-Rodriguez et al., 2009). In 2006, the FDA and the EMA issued alerts regarding the use of GBCAs in patients with renal insufficiency. The administration recommendations for GBCAs were subsequently modified, which led to a considerable decrease of new NSF cases (Bennett et al., 2012; EMA, 2010; FDA, 2006).

In the past two years, however, several new studies appeared, which provide evidence that gadolinium accumulates in the brain, bone, and kidneys of patients who were exposed to GBCAs, regardless of their renal function (Kanda et al., 2015; McDonald et al., 2017; Ramalho et al., 2016; Rogosnitzky and Branch, 2016). It is still not known whether it accumulates in its free or chelated form (Rogosnitzky and Branch, 2016). Besides NSF, GBCA administration was also found to cause acute, for instance nausea or anaphylaxia, and chronic or delayed adverse side effects. Table 4 provides an overview of reported adverse side effects not related to NSF observed after GBCA exposure in patients and model systems.

Table 4. GBCA-induced toxicity endpoints

Toxicity endpoints	Study type	Species/cells	Reference
Necrosis and apoptosis	*In vitro*	Renal tubular cells	(Heinrich et al., 2007)
Nephrotoxicity (reduced glomerular filtration rate)	*In vivo*	Pigs	(Elmstahl et al., 2006)
Nephrotoxicity (acute tubular necrosis)	Case report	Human	(Akgun et al., 2006)
Hematoxicity (reduced WBC count) Hepatotoxicity (vacuolar degeneration, disorganized hepatic cords)	*In vivo*	Mice	(Chen et al., 2015)
Pancreatitis	Case report	Human	(Blasco-Perrin et al., 2013)
Neurotoxicity (myoclonus, ataxia, tremor, and corpus callosum damage and hemorrhage)	*In vivo*	Rats	(Ray et al., 1996)
Neurotoxicity (encephalopathy)	Case report	Human	(Hui and Mullins, 2009)

WBC: White blood count. Table adapted from (Rogosnitzky and Branch, 2016)

1.6.1 GBCAs toxicity to the inner ear

Intratympanic application of GBCAs has been used as a standard procedure for the diagnosis of Meniere's diseases, see section 1.5.1.1. This raises the question whether there is a risk for GBCA-induced ototoxicity in patients exposed to GBCAs. Several *in vivo* and *in vitro* testing models have been used to characterize the effects of GBCAs on the inner ear, especially the sensory hair cells.

Effects on the stria vascularis

Intratympanic administration of eightfold diluted Omniscan had no toxic influence on the stria vascularis of the inner ear in guinea pigs. A higher concentration decreased the endocochlear potential and affected the marginal cells of the stria vascularis (Kakigi et al., 2008). In a separate study, Omniscan and Magnograf (also known as Magnevist)

were placed on the round window of guinea pig inner ears. Using electron microscopy, no alterations were observed in the stria vascularis (Suzuki et al., 2011).

<u>Effects on hair cells of the inner ear</u>

After intratympanic application of Omniscan in mice, mild hearing loss was detected using auditory brainstem response technique, while ProHance had no adverse effects in the same experiments (Nonoyama et al., 2016). In guinea pigs, no significant decrease in auditory brainstem response measurements was observed in experiments, where Omniscan was applied to the round window membrane of the inner ear (Duan et al., 2004). Similar results were obtained in an independent study (Zou et al., 2009). Using outer hair cells isolated from guinea pigs, a moderate morphological damage was found in 24% of the cells after administration of eightfold-diluted and in 3% of the cells with a sixteen-fold diluted ProHance®, a nonionic macrocyclic GBCA (Katahira et al., 2013).

In a study using isolated vestibular hair cells from bullfrogs, application of a four to sixteen-fold dilution of Omniscan led to morphological damage and reduced the frequency of action potentials in the semicircular canals, while 32-fold diluted Omniscan produced no obvious changes (Tanaka et al., 2010).

In 2007, Nakashima *et al.* succeed in visualizing ELH with three-dimensional fluid attenuated inversion recovery (3D-FLAIR) MRI in patients after intratympanic application of Omniscan. The authors did not report any adverse effects (Nakashima et al., 2007). Similarly, evaluation of treated patients failed detect any hearing loss one day after intratympanic administration of Magnograf (Louza et al., 2012). In a separate study with 65 MD patients, where the observation time was increased to one week, again no effects on audiologic control could be detected (Louza et al., 2013). Finally, a long term study with a follow-up at least six months after treatment showed no evidence of ototoxicity of intratympanic GBCA injection (Louza et al., 2015). Furthermore, to the best of our knowledge, there has been no report of GBCA-related intratympanic ototoxicity in the literature to date. Table 5 summarizes the key findings of the studies assessing ototoxicity mentioned above. Overall, the present evidence indicates little or no effects of intratympanic GBCA on hair cells of the inner ear. It is however not known, if all GBCAs have low ototoxicity.

Table 5. Selected studies assessing ototoxicity of GBCA exposure

Species	Compound	Dilution	Methodology	Toxic effects	Reference
Guinea pig	Omniscan	1	ABR	None	(Duan et al., 2004)
	Omniscan	1	ABR	None	(Zou et al., 2009)
	Omniscan, Magnevist (Magnograf)	1/8	Electron microscopy	None	(Suzuki et al., 2011)
	ProHance	1/8 - 1/16	OAE (distortion product evoked) microscopy	Moderate morphological damage	(Katahira et al., 2013)
Mouse	Omniscan, ProHance	1	ABR	Significant threshold decrease at 8 kHz with Omniscan; None observed with ProHance	(Nonoyama et al., 2016)
Bullfrog	Omniscan	1/4 - 1/32	AP recording after stimulation, Microscopy	Concentration-dependent morphological and physiological damages	(Tanaka et al., 2010)
Human	Omniscan	1/8		None	(Nakashima et al., 2007)
	Omniscan	1/8	Audiometry	None	(Louza et al., 2012)
	Omniscan	1/8	Audiometry	None	(Louza et al., 2013)
	Magnograf	1/8	Audiometry	None	(Louza et al., 2015)

Abbrevations: ABR, auditory brainstem response; AP, action potential; OAE, otoacoustic emissions. *None* indicates that no adverse side effects were observed.

1.7 Gentamicin and Its Application in MD Treatment

Gentamicin is a common aminocyclitol-aminoglycoside antibiotic with good effectiveness in gram-negative bacteria, but also in Staphylococcus and Mycobacterium tuberculosis. However, it can cause severe adverse side effects, mainly oto- and nephrotoxicity (Appel and Neu, 1978). The hearing damage is irreversible and it affects selectively the hair cells of the inner ear, most likely due to the high potential difference between the endolymph and these cells (Chen et al., 2014). Intratympanically applied gentamicin can destroy hair cells by diffusion via the round and oval window and is an ablative treatment method for a long-term control of vertigo in unilateral MD (Hsieh et al., 2009; Plontke et al., 2002). Due to the observed predilection of vestibulotoxicity over cochleotoxicity when applying Gentamicin, the vertigo can be reduced while hearing loss can be prevented in most cases (Plontke and Gurkov, 2015; Pullens and van Benthem, 2011).

1.8. Assessing Hair Cell Toxicity in *Xenopus* Embryos

In the present work, hair cells of the lateral line system of *Xenopus* embryos will be used to assess the potential ototoxicity of various GBCAs *in vivo*. The aminoglycoside antibiotic gentamicin will serve as a positive control, given its known toxicity to hair cells of the inner ear and the lateral line system. For example, the hair cell toxicity of gentamicin was assessed in *Xenopus* embryos by Stefan Schmitt in our laboratory in the context of his PhD thesis (Schmitt *et al.*, manuscript in preparation). Toxic effects of drug treatment on hair cells of the lateral line system can be visualized and quantitated by fluorescent microscopy. For this purpose, styryl pyridinium dyes such as FM1-43FX or DASPEI/DAPI are used to stain hair cells in the lateral line systems of zebrafish and *Xenopus* (Cochilla et al., 1999; Gale et al., 2001; Stengel et al., 2017)). Our laboratory found FM1-43FX to suit best for quantitatively measuring drug effects on hairs cells, as it features enormous staining ability and high selectivity (Schmitt *et al.*, manuscript in

preparation). FM1-43FX is a non-toxic water-soluble styryl pyridinium dye, which is unable to penetrate the lipid bilayer of membrane cells. It enters selectively hair cells by diffusion via the MET channels at the tips of the stereocilia and labels endosomes, mitochondria and rough endoplasmatic reticulum (Gale et al., 2001; Meyers et al., 2003; Nishikawa and Sasaki, 1996). The aliphatic amine group allows for aldehyde-based fixation through crosslinking, e.g. with formaldehyde (Fig. 10). Using FM1-43FX to stain hair cells of the lateral line system after GBCA treatment, the *in vivo* toxicity of GBCAs will be established in a comparative manner under established standard conditions.

FM1-43FX

$$H_3N^+(CH_2)_3\overset{\overset{\displaystyle CH_3}{|}}{\underset{\underset{\displaystyle CH_3}{|}}{N^+}}(CH_2)_3\overset{+}{N} \text{—} CH=CH \text{—} N[(CH_2)_3CH_3]_2 \quad 3\,Cl^-$$
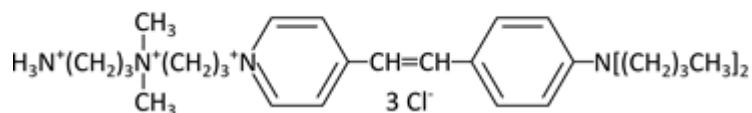
Fig. 10. Structure of FM1-43FX. The fluorescent dye FM1-43FX, ((n-(3-aminopropyldiethylammoniumpropyl)-4-(dibutylamino)-styryl) pyridinium tri-chloride, contains a fluorescent styrylpyridinium moiety (right) and an aliphatic amine group (left).

2 AIMS OF THE STUDY

The general goal of the present study was the assessment of the safety of GBCAs for hair cells, which are the sensory cells of the auditory and vestibular organs of the body. Five compounds representing four distinct classes of GBCAs were selected for comparative characterization. *In vivo* toxicity testing was performed using the hair cells of the lateral line system of the *Xenopus* embryo. Using a standardized *in vivo* test system, the following specific aims were defined:

- To carry out dose-dependent treatments of *Xenopus* embryos with waterborne GBCAs and monitor their effects on hair cells of the lateral line system
- To establish quantitative hair cell toxicity parameters, *i.e.* EC_{50} values
- To assess the overall toxicities of GBCAs for *Xenopus* embryos, *i.e.* LC_{50} values
- To compare the hair cell toxicity parameters established for GBCAs in *Xenopus* with those determined using other animal models and in human patient studies
- To formulate recommendations regarding the safety of GBCAs for intratympanic applications

3 MATERIALS AND METHODS

3.1 *In vitro* Fertilization and Culture of *Xenopus* Embryos

Adult *Xenopus laevis* frogs were purchased from Nasco, Fort Atkinson, WI, USA and *Xenopus* Express, Vernassal, France. *Xenopus* males and females were kept separated from each other in 72-l, 170-l, and 200-l tanks filled with tap water and supplemented with common table salt and enrichments, according to the German animal welfare regulations. The water temperature was between 18°C and 20°C. The animals were held on 24-h day/night cycle with a 12-h day period. They were fed with food pellets (TabiMin, Tetra). The experimental procedures using *Xenopus* frogs were approved by the Regierung von Oberbayern, Munich, Germany (Permit 55.2-1-54-2531.6-3-10).

3.1.1 *In vitro* fertilization

In vitro fertilizations were performed to obtain *Xenopus* embryos that were developing synchronously. *Xenopus* females were primed with 350 to 1000 IU of hCG injected subcutaneous to induce ovulation. After incubation of 12 to 16 hours at 18°C, injected females were gently massaged to facilitate egg laying. Testes for *in vitro* fertilizations were dissected from the fatty body of sexual maturated *Xenopus* males, which had been subjected to lethal anesthesia using Tricaine mesylate (MS-222). Isolated testes were washed with PBS and transferred to testes medium for storage at 4°C. To initiate *in vitro* fertilization, freshly obtained eggs were covered with piece of testis macerated in 1 ml 1x MMR. After 5 min, 0.1x MMR was added and the fertilized eggs were incubated at 20°C. The jelly coats of cleavage stage embryos were dissolved by treatment with freshly prepared 2% cysteine solution. Dejellied embryos were extensively washed with 0.1x MMR.

3.1.2 Culture of Embryos

Groups of about 100 embryos were transferred with a plastic pipette to 5-cm Petri dishes and cultured in 0.1 x MMR at 20°C. The embryo cultures were checked regularly. Dead embryos and those with developmental abnormalities were removed. The medium was

changed daily. Embryos were staged according to at Nieuwkoop and Faber (Nieuwkoop and Faber, 1967).

3.2 Assessment of Hair Cell Toxicity in *Xenopus* Embryos

The assessment of hair cell toxicity was based on a standardized method established by S. M. Schmitt in the laboratory (S. Schmitt *et al.*, manuscript in preparation). The *in vivo* test system permits the rapid and quantitative assessment of toxicity of waterborne drugs for hair cells of the lateral line system of *Xenopus* embryos. Five GBCAs were selected for testing: Omniscan, Magnograf, MultiHance, Dotarem, and Gadovist. Gentamicin and gadolinium served as positive controls. Each compound was assessed in at least three independent experiments using clutches from three different *Xenopus* females.

3.2.1 Experimental setup

48-well polystyrene microplates with 1.6 ml-volume well were used for embryo testing. Baskets to accommodate the embryos were homemade from 1.5 ml Eppendorf tubes as follows. The cap and the bottom of the Eppendorf tube were cut off using a sharp scalpel. Heat-stable nylon net (mesh) filters (100 μm pore size) was fused by heating at 160°C to the bottom of the tube to creating a basket with perforated bottom (Fig. 12A). Each compound was tested at seven different concentrations. The test concentrations were as follows: 1 mM, 2 mM, 5 mM, 10 mM, 20 mM, 50 mM, and 100 mM. The dilutions were prepared in 1.5-ml Eppendorf tubes with 0.1 x MMR right before testing. Opened contrast agent bottles were sealed with Parafilm and stored under light protection at 4°C. Gadolinium trichloride dilutions were prepared freshly every time. Gadolinium trichloride was tested at 0.5 μM, 1 μM, 2 μM, 5 μM, 10 μM, 20 μM, and 50 μM. Gentamicin dilutions were prepared from a 10 x stock solution (10 mg/ml), which was stored at 4°C. The following concentrations were tested: 0.1 μg/ml, 0.2 μg/ml, 0.5 μg/ml, 1 μg/ml, 2 μg/ml, 5μg/ml, and 10 μg/ml.

The 48-well microplates were prepared by transferring 0.8 ml of each dilution and dispensing the dilution to the wells as shown in Fig. 11.
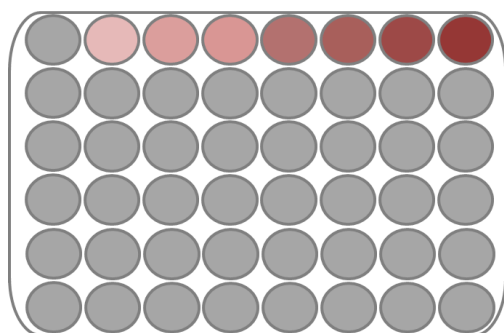

Fig. 11. Schematic illustration of a 48-well microplate used for compound testing. Grey wells contain 0.8 ml of culture medium (0.1 x MMR). Wells shown with increasing degrees of red indicate wells filled with 0.8 ml of compound solution representing increasing compound concentrations.

This described experimental setup was designed to enable efficient execution of the experimental procedures. For example, the setup with baskets harboring the embryos allows for easy, fast, and standardized treatments and the embryos in the baskets can be rapid moved to new wells for washing purposes (Fig. 12B).
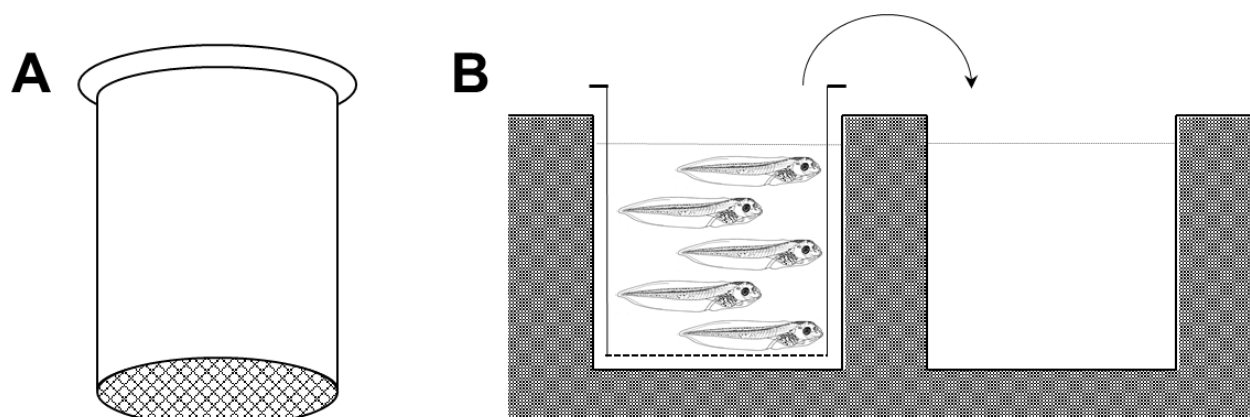

Fig. 12: Using basket to transfer embryos from one well to another. A: Side view of a custom-made basket with a Nylon mesh filter fused to the bottom. **B**: Transfer a basket with embryos from one well to a new one.

3.2.2 Compound treatments

Embryos at stage 41 (4 days post fertilization at 20°C) were selected for compound treatment. Appropriate compound dilutions were dispensed as outlined in Fig. 11. The homemade baskets were then placed into a 48-well microplate. Five stage 41 embryos were added into each baskets and incubated at 22°C for 24 hours. The most left well contained 0.1 x MMR and those embryos served as controls. Evaporation was

minimized by covering the microplates with a plastic lid and carrying out the incubations in a humidified incubator.

3.2.3 Labeling and fixation

After 24 hours of incubation, the embryos have reached stage 45. The baskets were transferred to wells filled with 0.1 x MMR for 5 min to stop the treatment and to wash the embryos. This step was repeated one more time to further reduce the exposure to the compound.

For fluorescent labeling, a 2-mM stock solution was prepared by dissolving 100 µg FM1-34FX in 89 µl DMSO and 22-µl aliquots were stored at -20°C in the dark. Under protection from light, an aliquot was dissolved in 0.1 x MMR to a final concentration of 2 µM. 0.8 ml of labeling solution was dispensed to each well shortly before embryo staining was initiated. During and after labeling the embryos were kept protected from day light. After precisely 5 min of fluorescent labeling with FM1-34FX at room temperature, the baskets containing the embryos were transferred to fresh wells containing in 0.1 x MMR for 5 minutes of washing. The washing step was repeated one more time before the embryos were fixed with in freshly prepared MEMFA for 45 min on a horizontal shaker. For fixation, the embryos were transferred from baskets to wells containing MEMFA to provide them more space and to prevent fixation of bent or twisted embryos. Fixed embryos were transferred into PBS/EDTA and stored in the dark until they were used for imaging. The entire treatment procedure is summarized and illustrated in Fig. 13.
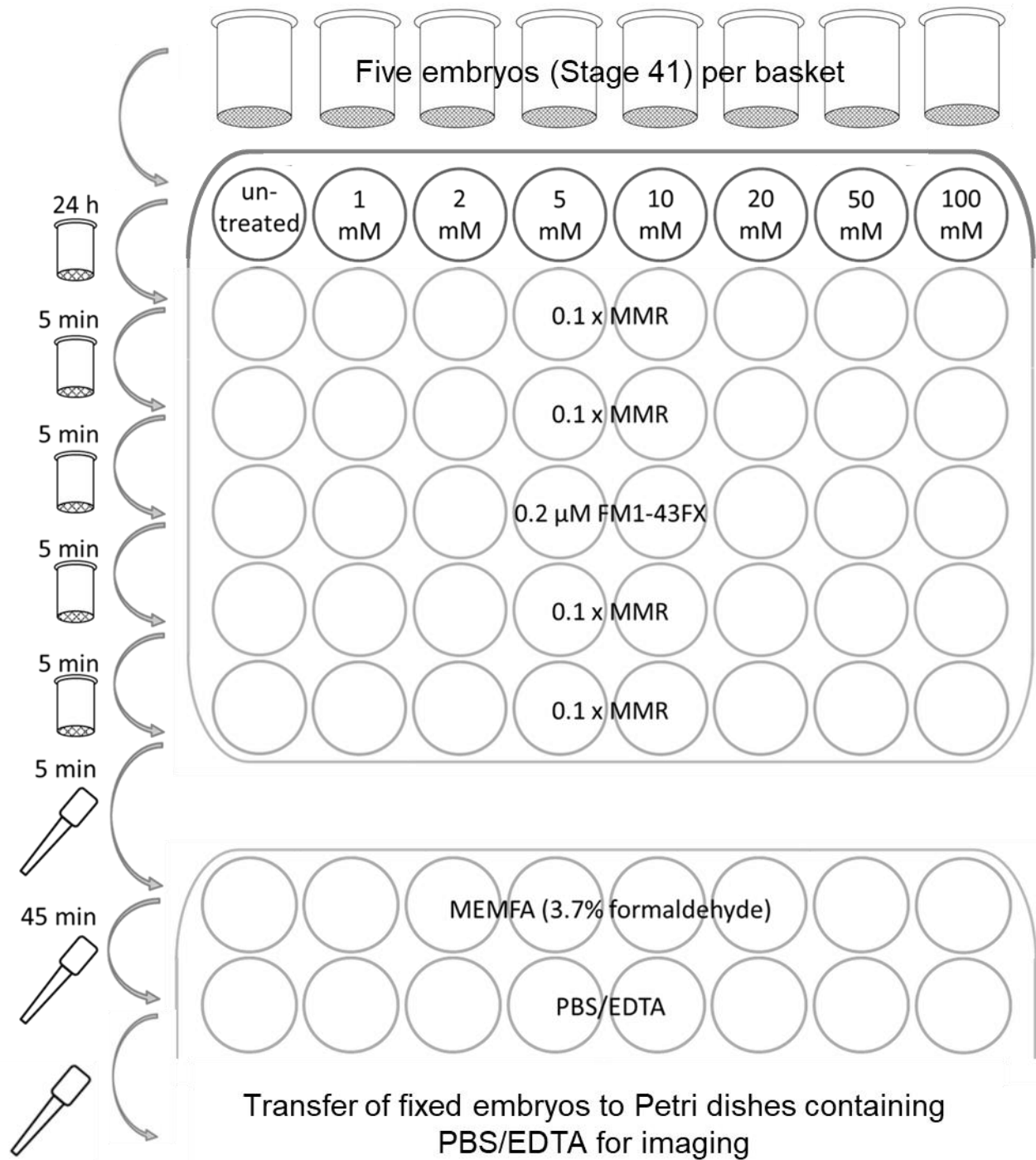
Fig. 13. Visualization of the treatment procedure to assess of the hair cell toxicity of GBCAs in *Xenopus* embryos. Baskets were supplemented with five stage-41 embryos each and transferred.to the 48-well dish. After the indicated incubation times, the embryos were transferred to the next row of wells either in the baskets or using a plastic pipette as shown.

3.2.4 Imaging of fluorescently labeled embryos

The embryos were transferred to glass Petri dishes coated with PBS/EDTA-agarose and covered by PBS/EDTA. Small wells were scratched into the agarose to facilitate lateral positioning of the embryos for imaging. A Leica M205 FA fluorescence stereomicroscope was used to image the fluorescently labeled hair cells. Excitation and emission were detected with the Leica-GFP filter set (excitation filter: 470 nm/40 nm; Emission Filter: 525 nm/50 nm). From each embryo, a Z-stack consisting of 28 single pictures was generated. The Z-stack has covered an 810 μm of depth at a magnification of 24x and an exposure time of 192 ms. Each Z-stack was used to generate a single picture of each embryo using the Leica Application Suite (LAS) X software platform.

3.2.5 Image processing and quantitation of fluorescence

The image processing program Image J (Version 1.47; Wayne Rasband, NIH, USA) was used for the quantitative evaluation of the fluorescence intensity (FI). The picture files were opened using Image J, the RGB channels were split, and the channel "green" was selected. The analysis was restricted to the dorsolateral region of the lateral line system as shown in Fig. 14. This decision was based on the fact that (i) less natural variation between different embryos was observed for the dorsolateral lateral line system, and (ii) the dorsolateral part of the lateral line system is easier to image as it is located in flatter area of the embryo. The threshold for the fluorescence signals was set to 9000 until infinity. The area of interest was analyzed and data for size of stained area, mean value, minimum, maximum, and median fluorescence values were calculated.
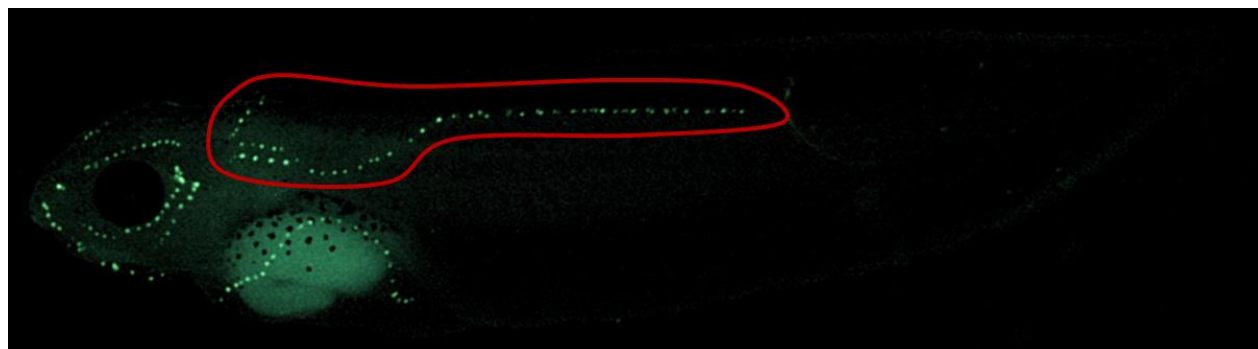
Fig. 14. Example of a *Xenopus* embryo at stage 45 after FM1-43FX labeling. The area of the lateral line system used for quantitation purposes is outlined in red.

3.2.6 Statistical evaluation

The raw data obtained for each embryo was transferred to Microsoft Excel software (Microsoft Excel 2010 V14.0, Microsoft, USA). The mean value of fluorescence was multiplied by the size of the stained area to calculate the FI for each embryo as follows:

$$FI = mean\ fluorescence\ x\ size\ of\ area$$

The mean value and the standard deviation of the FI was calculated using all five embryos treated with the same compound concentration. If an embryo was not in the triple standard deviation confidence interval of the others ($\sigma \leq -3$ or $\sigma \geq 3$), it was assumed that the embryo was with a probability of 99.7% an outlier. Hence, it was excluded from the analysis. Only one outlier per compound concentration tested was tolerated. Otherwise, the entire 48-well dish was excluded and the experiment was repeated.

Standardization of the FI values for each experimental set (*i.e.* 48-well dish) was necessary to permit a qualified statement about the impact of compounds on hair cell survival. The following formula was applied to the fluorescence intensity values:

$$RFU\ [\%] = FI_{[treated]}\ /\ FI_{[untreated]}\ x\ 100$$

where, RFU indicates relative fluorescence unit; $FI_{[treated]}$ means the mean value of FI of all five embryos for a particular compound concentration tested; $FI_{[untreated]}$ refers to the mean value of FI of the five untreated control embryos.

Setting the value of the untreated controls to 100% allowed (i) to bring the treated embryos for a given compound concentration into a standardized relation to the untreated control and (ii) to compare the results of all experiments between each other.

To visualize the results, the calculated values were transferred to the statistics and graphing software SigmaPlot (SigmaPlot 12, Systat Software Inc., USA). The graph shown for each compound tested is composed from data obtained from three independent experiments. Mean values and standard deviations of the RFU were visualized using scatter and line graph with error bars.

The EC_{50} value is defined here as the effective concentration reducing the RFU to 50%. EC_{50} values were calculated with SigmaPlot by fitting a sigmoidal curve using a four-parameter logistic curve algorithm. The statistical significance tests were performed through using ANOVA (Analyze of Variance) in SigmaPlot. The raw FI data for each embryo was compared to the others of the same experiment by One-Way-Analysis-of-Variance. Significance level was defined as ($p < 0.05$).

3.3 Assessment of Adverse Side Effects of GBCAs on *Xenopus* Embryogenesis

The development of *Xenopus* embryos during contrast agent exposure was observed for five days to determine possible adverse side effects (ASE). The five contrast agents (Omniscan, Magnograf, MultiHance, Dotarem, and Gadovist) and gadolinium trichloride were assessed. Each compound was tested in three independent experiments using embryos from at least three different *Xenopus* females.

3.3.1 Preparation of multiwell dishes

The dilutions of the test compounds were prepared right before starting the treatments. The dilutions were made in 1.5-ml Eppendorf tubes using 0.1 x MMR. The embryos were treated with the dilutions in 48-well dishes. Each well contained 1 ml compound solution. Contrast agents and gadolinium trichloride were tested at seven different concentrations. GBCAs were tested at 1 mM, 2 mM, 5 mM, 10 mM, 20 mM, 50 mM, and 100 mM (as in the hair cell toxicity assays above). Gadolinium trichloride was tested at final concentrations of 10 μM, 20 μM, 50 μM, 100 μM, 200 μM, 500 μM, and 1 mM. Control embryos were treated with 0.1 x MMR.

3.3.2 Compound treatment

Healthy normal embryos at stage 31 (2 days post fertilization at 20°C) were selected and washed in 0.1 x MMR. Five embryos were transferred to each well for compound testing. The multiwell dishes with the embryos were incubated at 22°C. To minimize evaporation, all wells that did not carry embryos were filled with 0.1 x MMR, the multiwell plates were covered with a lid, and they were transferred to an air humidified incubator.

The development of the embryos was checked twice a day when embryos reached the following embryonic stages: 33/34, 37/38, 39, 40, 41, 42, 43, 44, 45, 46, and 47. The experiments were terminated about 7 days post fertilization. The embryos were inspected to determine whether compound treatment caused developmental delays, externally visible abnormalities, or lethality. Any abnormal effects were documented. Dead embryos were removed from the well as soon as they were detected.

3.3.3 Statistical evaluation

Mean values and the standard deviations for pools of five embryos per well were calculated using Microsoft Excel software. These values were transferred to Sigmaplot and used to generate 3D Mesh plots, with embryonic stages, compound concentrations, and the observed abnormality (lethality) representing one of the three axes each. To simplify the illustrations, the mean values of the three surveys of every compound were used without plotting the standard deviation. Hence, no error bars are shown. LC_{50} is defined as the lethal concentration causing death of 50% of the treated embryos. Stage 45 was chosen as the endpoint to calculate of the LC_{50} values. Line and scatter graph were generated with error bars. Sigmaplot calculated the LC_{50} value by fitting a sigmoidal curve to the stage 45 graphs using a four-parameter logistic curve algorithm.

3.4 Materials

Table 6. Test compounds

Name	Supplier	Batch number (lot)
Gadodiamide Gd-DTPA-BMA (Omniscan®) 0.5 M gadolinium(III) 5,8-bis(carboxylatomethyl)-2-[2-(methylamino)-2-oxoethyl]-10-oxo-2,5,8,11-tetraazado-decane-1-carboxylate hydrate	GEHealthcare	11406948 12447313

Gadopentetate-Dimeglumine Gd-DTPA (Magnograf®) 0.5 M gadolinium(III) 2-[bis[2-[carboxylatomethyl (carboxymethyl)amino]ethyl]amino]acetate	Marotrast	93090J 21125J
Gadobenate-Dimeglumine Gd-BOPTA (MultiHance®) 0.5 M gadolinium(III) 2-[2-[carboxylatomethyl-[2- [carboxylatomethyl(carboxymethyl)amino] ethyl]amino]ethyl-(carboxymethyl)amino]-3- phenylmethoxypropanoate	Bracco Imaging	S2P274C S4P253C
Gadoterate-Meglumine Gd-DOTA (Dotarem®) 0.5 M gadolinium(III)2-[4,7,10-tris(carboxymethyl)- 1,4,7,10-tetrazacyclododec-1-yl]acetate	Guerbet	13GD001B
Gadobutrol Gd-DO3A-Butrol (Gadovist®) 1 M gadolinium(III) 2,2′,2"-(10-((2R,3S)-1,3,4- trihydroxybutan-2 yl)1,4,7,10 tetraazacyclododecane-1,4,7-triyl)triacetate	Bayer	24792A 42805B
Gentamicin 10 mg/ml	Gibco	1142800
Gadolinium Gadolinium(III)-chloride hexahydrate	Sigma-Aldrich	SLBG7250V SLBD9588V

Table 7. Reagents

Name	Supplier	Batch number (lot)
Aqua ad iniectabilia	Braun	
Cysteine Solution: 2% L-Cysteine in H_2O solution, pH 7.8 (adjusted with 10 x NaOH)		
Dimethyl sulfoxide (DMSO) Hybri-Max®	Sigma-Aldrich	D2650
EDTA: 0.5 M EDTA, pH 8.0 (adjusted with NaOH)	AppliChem	A2937

EGTA: 0.5 M EGTA, pH 8.0 (adjusted with NaOH)	AppliChem	A0878
Fetal calf serum	Gibco	10110-153
FM®1-43FX: 2 mM FM1-34FX in DMSO, stored at -20°C	Invitrogen	F35355
Formaldehyde-solution 37%	AppliChem	A0877
HEPES	AppliChem	A1069
Human Chorionic Gonadotropin (hCG): 2000 IU/ml hCG in H_2O	Sigma-Aldrich	CG-10
Hydrochloric acid 32%	AppliChem	A2078
Magnesium sulfate heptahydrate	Fluka	63140
1 x Marc's modified Ringer Solution (MMR): 100 mM NaCl, 2 mM KCl, 2 mM $CaCl_2$, 1 mM $MgSO_4$, 5 mM HEPES, pH 7.8		
0.1 x MMR: 1:10 dilution of 1 x MMR		
10 x MOPS/EGTA/Magnesium Sulfate (MEM salts): 1 M MOPS, 20 mM EGTA, 10 mM MgSO4, pH 7.4, stored at 4°C, protected from light		
1 x MOPS/EGTA/Magnesium Sulfate/Formaldehyde Buffer (MEMFA): 1:10 dilution of MEM salts, 3.7% Formaldehyde		
MOPS	AppliChem	A1076
1 x Phosphate Buffered Saline/EDTA (PBS/EDTA): 1 M PBS, 10 mM EDTA, pH 7.4		
PBS/EDTA-Agarose: 1 M PBS, 10 mM EDTA, 2% Agarose		
Phosphate Buffered Saline 10x pH 7.4	GIBCO	70011
Potassium chloride	AppliChem	A2939

Sodium chloride	AppliChem	A4661
Sodium Hydroxide 10N	VWR	310933
Testes Medium: 1 x MMR, 10% fetal calf serum, 2% gentamicin, sterilized by filtration (0.45 µm filter), stored at -20°C		
Tricaine mesylate	Sigma-Aldrich	A5040
Ultra-Pure ᵀᴹ Agarose	Invitrogen	16500

Table 8. Tools and Instrumentation

Name	Supplier	Batch number (lot)
COSTAR® 48 Well Plate	Corning	3548
Leica M205 FA Fluorescence Stereomicroscope	Leica	M205 FA
Microtubes 1.5 ml EASY CAP Plastic pipette	SARSTEDT	72.690.550
NYLON NET FILTERS – 100 µm NY1H	Millipore	NY1H02500
Plastic Petri dishes	Greiner bio-one	663102

4 RESULTS

4.1 Assessing the Hair Cell Toxicity of GBCAs

The hair cells of the *Xenopus* lateral line system served as a convenient *in vivo* test system to assess the toxic effects of GBCAs. Five GBCAs approved for use in humans were selected for testing: Gadodiamide (Omniscan®), Gadobutrol (Gadovist®), Gadobenate Dimeglumine (MultiHance®), Gadoterate Meglumine (Dotarem®), and Gadopentetate Dimeglumine (Magnograf®). Compounds with known hair cell toxicities, such as gadolinium and the aminoglycoside antibiotic gentamicin, served as positive controls. Embryos simply incubated in the culture medium (0.1 x MMR) were used as negative controls. *Xenopus* embryos were treated in 48-well microplates with GBCA concentrations ranging from 1 mM to 100 mM for 24 hours at 22°C. Subsequently, the hair cells were labeled with the fluorescent dye FM1-43FX and fixed in MEMFA. Loss of fluorescent labeling correlates with compound-induced damage to hair cells. Hence, the fluorescence intensity (FI) was quantified after microscopic imaging. Every compound was tested with five embryos per well at each concentration in at least three independent experiments.

4.2 Free Gadolinium Shows Considerable Hair Cell Toxicity

Gadolinium trichloride hexahydrate, a colorless, hygroscopic, water-soluble compound, was used as a source for free gadolinium. Gadolinium treatment of *Xenopus* embryos resulted in a concentration-dependent decrease of fluorescent staining of hair cells, indicating toxicity of the compound (Fig. 15). At a gadolinium concentration of 5 µM, the lateral line system appeared to be widely damaged, and the treatment with 50 µM almost completely destroyed the lateral line. There were no other morphological abnormalities identifiable in the treated embryos. Fig. 16 shows the quantitative analysis of the fluorescence associated with the hair cells of the dorsolateral aspects of the

lateral line system. The obtained dose-response curve demonstrated that RFU declined to nearly zero at gadolinium concentrations of 50 µM and higher with an estimated EC_{50} value of 9.7 µM.
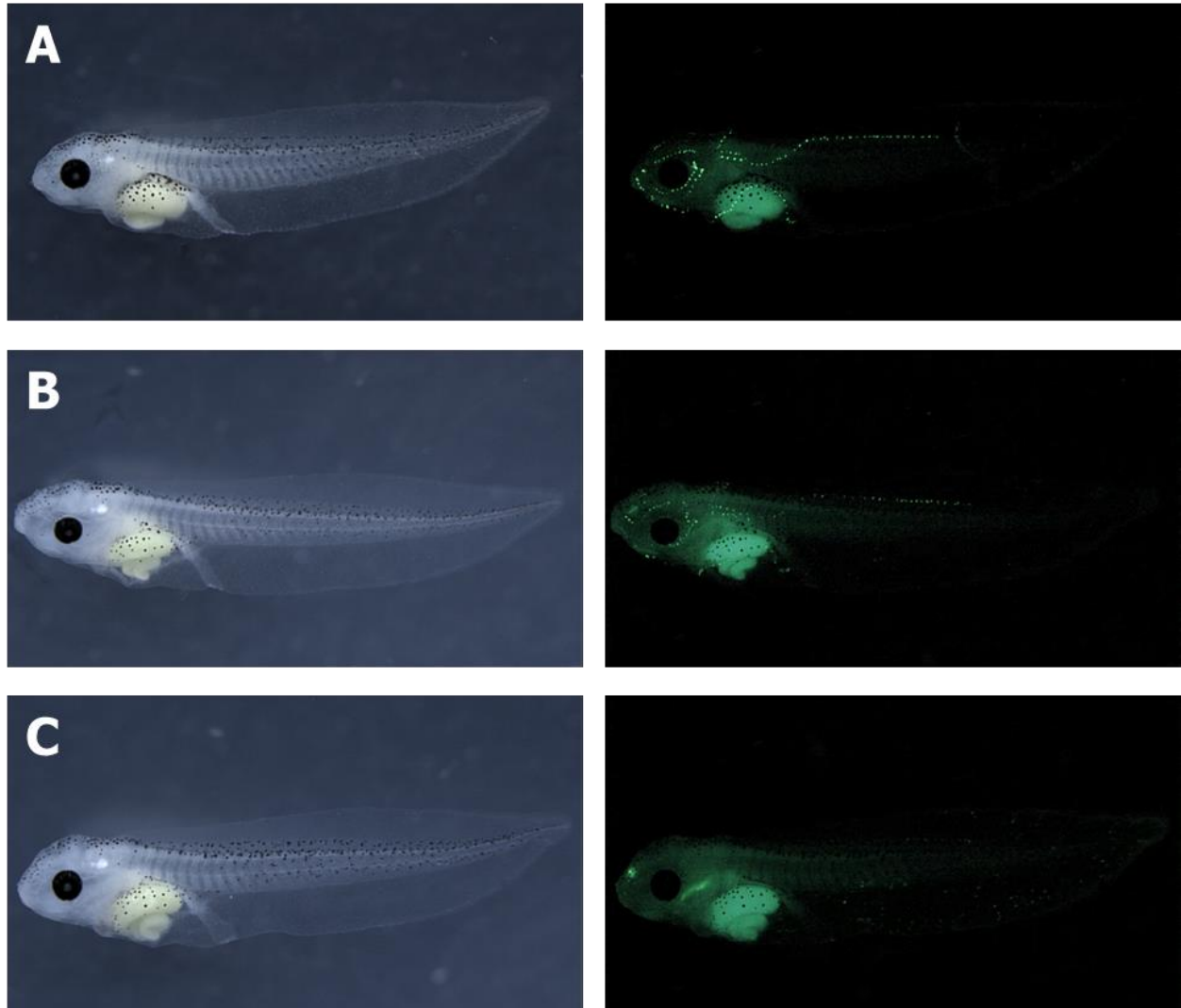

Fig. 15. Treatment of *Xenopus* embryos with gadolinium trichloride. The embryos were treated for 24 hours with the compound and subsequently labeled with FM1-43FX**.** Brightfield images are shown on the left with corresponding fluorescent ones on the right. **A**: Control untreated embryo; **B, C**: Representative embryos treated with 5 µM (**B**) and 50 µM (**C**) gadolinium trichloride.

Gadolinium trichloride
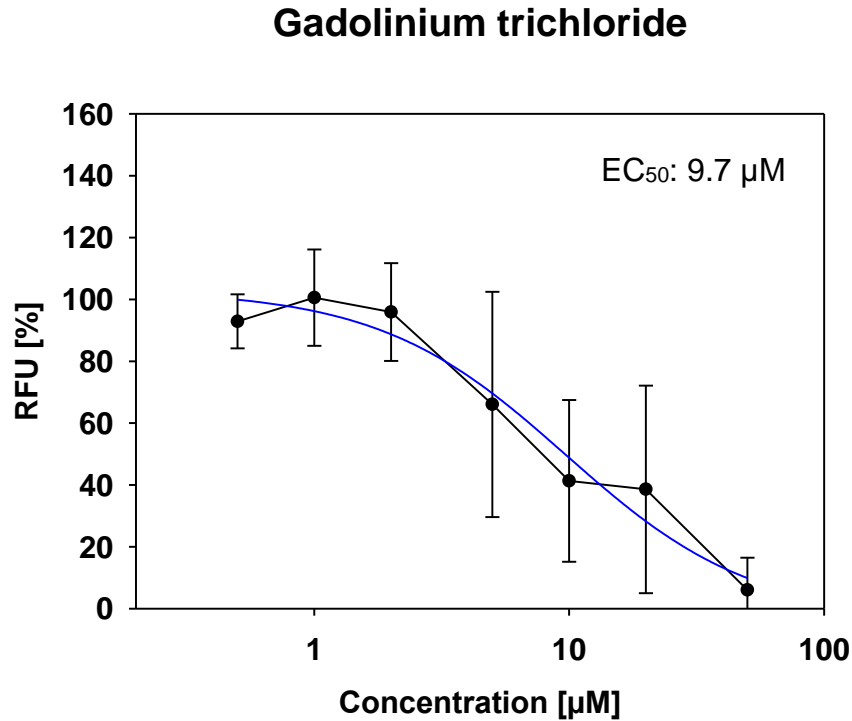
Fig. 16. Dose-response curve relating the gadolinium trichloride concentration to the fluorescent staining of lateral line hair cells. Fluorescent staining was performed after 24 hours of gadolinium treatment. Mean values and standard deviations (*error bars*) are shown (*n*=3). Statistical evaluation and significance calculations were done using SigmaPlot. Nonlinear regression with a four-parameter logistic curve (blue) was used to calculate of indicated EC_{50} value.

4.3 Gentamicin and Gadolinium have Comparable Hair Cell Toxicities

The aminoglycoside gentamicin is known for its toxicity towards hair cells of the lateral line system. We therefore asked how its toxicity compares to that of gadolinium. As shown in Fig. 17, gentamicin treatment reduced fluorescent staining of hair cells in a concentration-dependent manner towards zero. The calculated EC_{50} value was 0.96 µg/ml, which is approximately 2.01 µM. In summary, both gadolinium and gentamicin induce hair cell toxicity at concentrations in the low µM range.

.
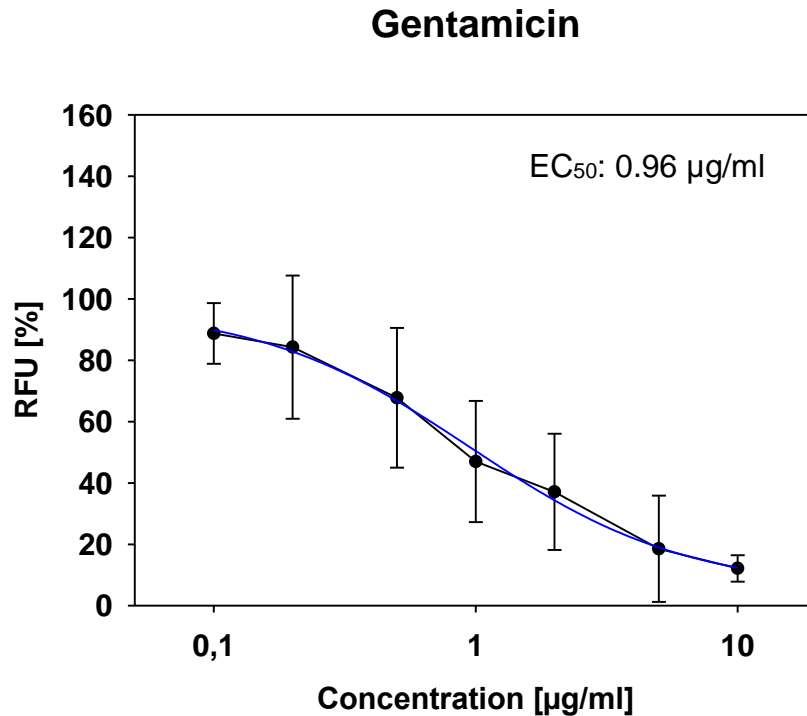
Gentamicin

Fig. 17. Dose-response curve relating the gentamicin concentration to the fluorescent staining of lateral line hair cells. Fluorescent staining was performed after 24 hours of gentamicin treatment. Mean values and standard deviations (error bars) are shown (n=3). Statistical evaluation and significance calculations were done using SigmaPlot. Nonlinear regression with a four-parameter logistic curve (blue) was used to calculate the indicated EC50 value.

4.4 Differential Effects of GBCAs on Hair Cells of *Xenopus* Embryos

The assessment of the toxicity of GBCAs for the hair cells of the lateral line system of *Xenopus* embryos resulted in no or only very moderate loss of RFU over the concentrations tested (**Fehler! Verweisquelle konnte nicht gefunden werden.**). Importantly, these concentrations were 2000-fold higher than those used to test gadolinium (100 mM vs 50 µM). Overall, the mean RFU values obtained for the different GBCAs after embryo treatment never declined below half of control RFU. Nevertheless, interesting differences between the toxicities of the GBCAs were noticeable. While Omniscan and Gadovist displayed little to no toxicities for *Xenopus* lateral line hair cells,

moderate but statically significant loss of fluorescent staining was observed after treatment with Dotarem and Magnograf. Unexpectedly, the latter and MultiHance were found to be lethal for the embryos at 100 mM, the highest concentration tested over the 24-hour incubation period in three independent experiments.
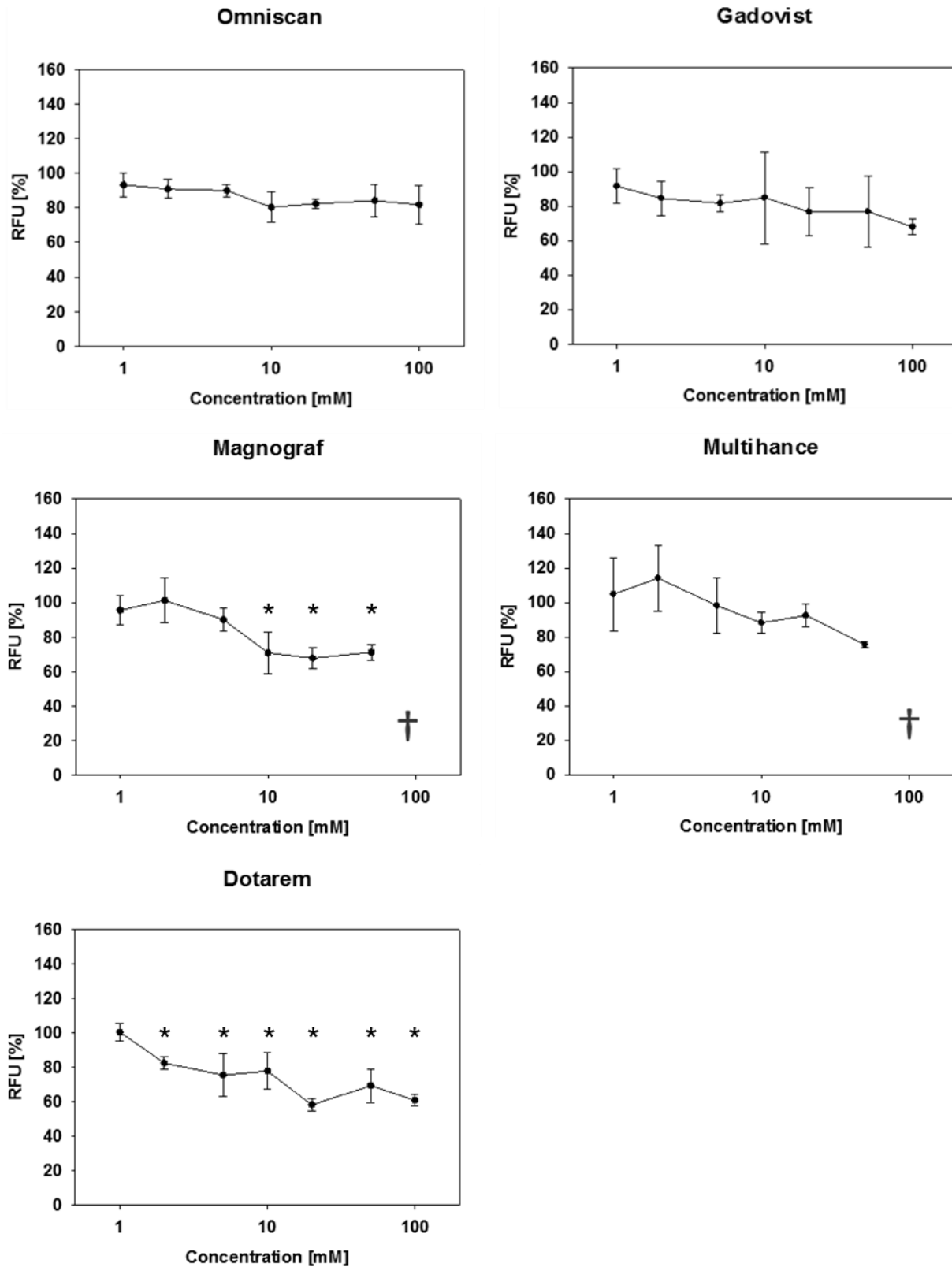
Fig. 18. Dose-response curves relating GBCA concentrations to the fluorescent staining of Xenopus lateral line hair cells. Fluorescent staining was performed after 24 hours of GBCA

treatment. Mean values and standard deviations (error bars) are shown. Asterisks indicate significance with p>0.05. At 100 mM, Magnograf and Multihance cause embryonic lethality within 24 hours. Statistical evaluation and significance calculations were done using SigmaPlot. All tested compounds passed normality and equal valiance test.

4.5 Assessing the Effects of GBCA Treatment on *Xenopus* Embryogenesis

As mentioned above, treatment of *Xenopus* embryos with Magnograf or MultiHance at a final concentration of 100 mM was lethal for the embryos within 24 hours of incubation. These findings raised the question whether prolonged treatment with GBCAs had any adverse effects on *Xenopus* embryogenesis. Furthermore, the concentrations causing lethality in 50% of the embryos (LC_{50}) were to be established, where appropriate. Gadolinium and the five GBCAs were used to monitor their effects on *Xenopus* embryogenesis between stage 31 to 47, covering a period of five days at 20 °C. Dose-response studies were performed in 48-well dishes with five embryos per well. Control wells contained embryos in 0.1 x MMR only. The embryos were inspected every 12 hours using a stereomicroscope for any externally discernible malformations or phenotypes. Each compound was tested in three independent experiments with comparable results.

4.6 Gadolinium Treatment Causes Embryonic Lethality

Gadolinium trichloride treatments were performed with concentrations ranging from 10 to 1000 µM. Embryonic lethality was observed at 20 µM and higher concentrations. At 100 µM, the embryos reached stage 41 before they started to die, whereas embryos died immediately after exposure to a concentration of 1000 µM. Using stage 45 as an endpoint, a LC_{50} value of 56.7 µM was estimated (Fig. 19).
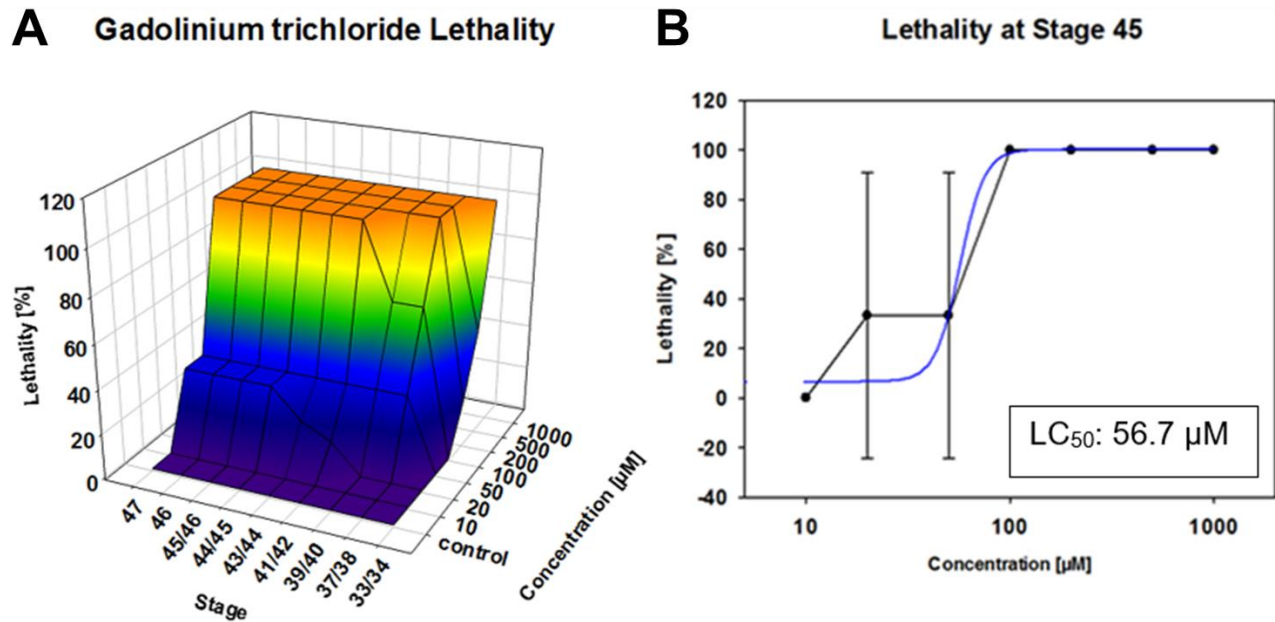
Fig. 19. Lethality of *Xenopus* embryos occurring during gadolinium trichloride treatment. A: 3D-Mesh-Plot of embryonic lethality, stage, and concentration (*n*=3) **B:** Line and scatter plot of lethality at stage 45.

4.7 Differential Effects of GBCA Treatments on *Xenopus* Embryogenesis

Xenopus embryos were treated with GBCAs at concentrations ranging from 1 mM to 100 mM. Treated embryos were not only scored for lethality, but also inspected for hemorrhages, edema, and other visible abnormalities. Significant differences were observed between the GBCAs studied here. Omniscan treatment even at the highest concentration of 100 mM had no obvious effects on *Xenopus* embryogenesis as shown in Fig. 20.
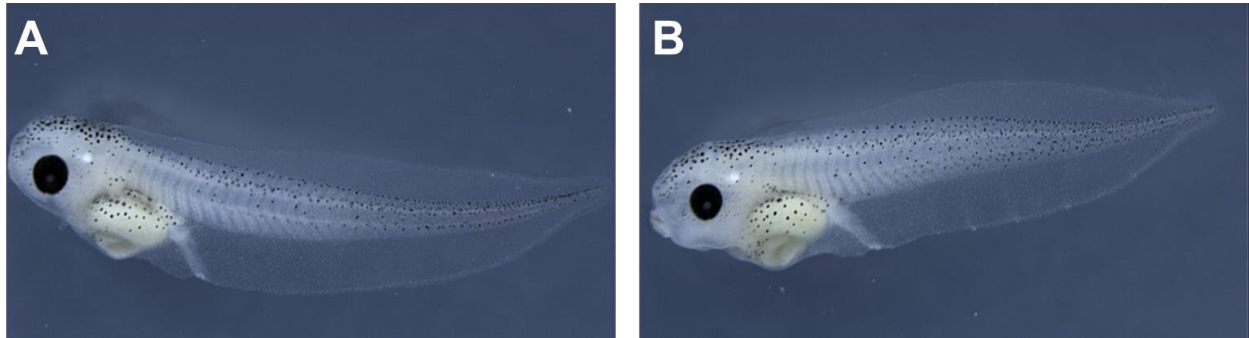
Fig. 20. Wild-type phenotype observed with Xenopus embryos at stage 45 after 72 hours of treatment with 100 mM Omniscan. A: Control embryo. **B**: Embryo treated with 100 mM Omniscan.

By contrast, treatment of *Xenopus* embryos with 100 mM Magnograf caused lethality after 24 hours (**Fehler! Verweisquelle konnte nicht gefunden werden.**). Before dying, the embryos often displayed developmental delays and reduced swimming activity (not shown).

Fig. 21. Appearance of a dead *Xenopus* embryo observed 24 hours after treatment with 100 mM Magnograf.

Besides Omniscan, Gadovist treatment had also no detectable effects on *Xenopus* embryogenesis as documented in Fig. 22 and Fig. 23, respectively.
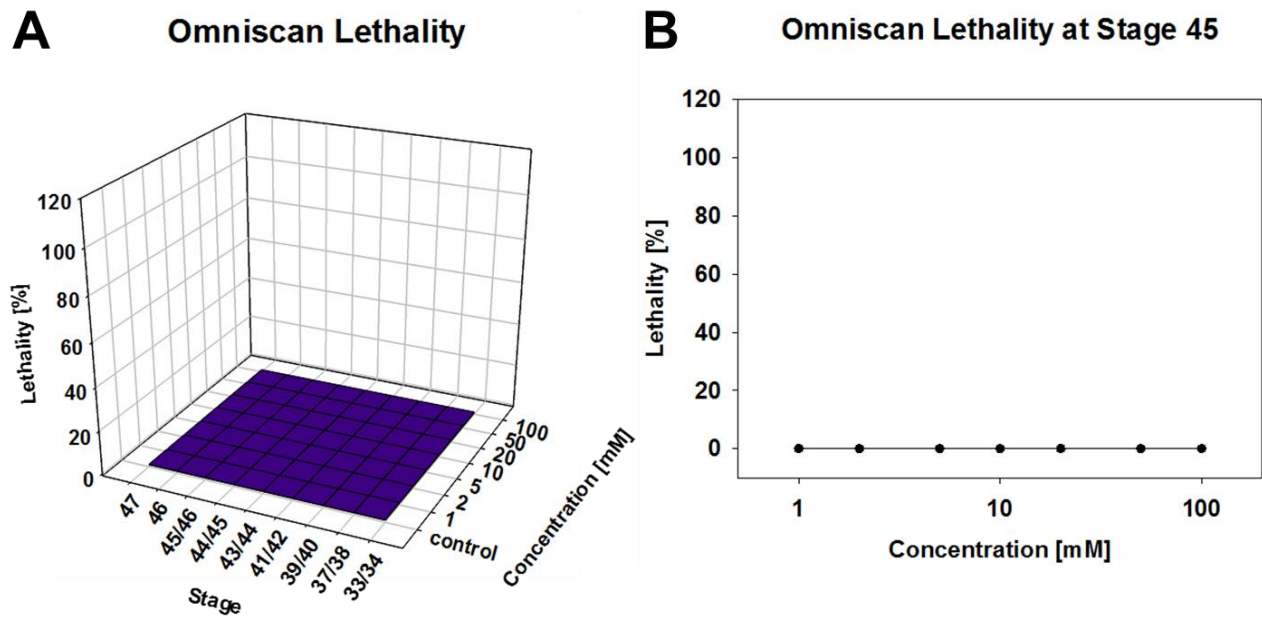
Fig. 22. Absence of lethality in *Xenopus* embryos treated with Omniscan. A: 3D-Mesh-Plot of embryonic lethality, stage, and concentration (*n*=3) B: Line and scatter plot of observed lethality at stage 45.
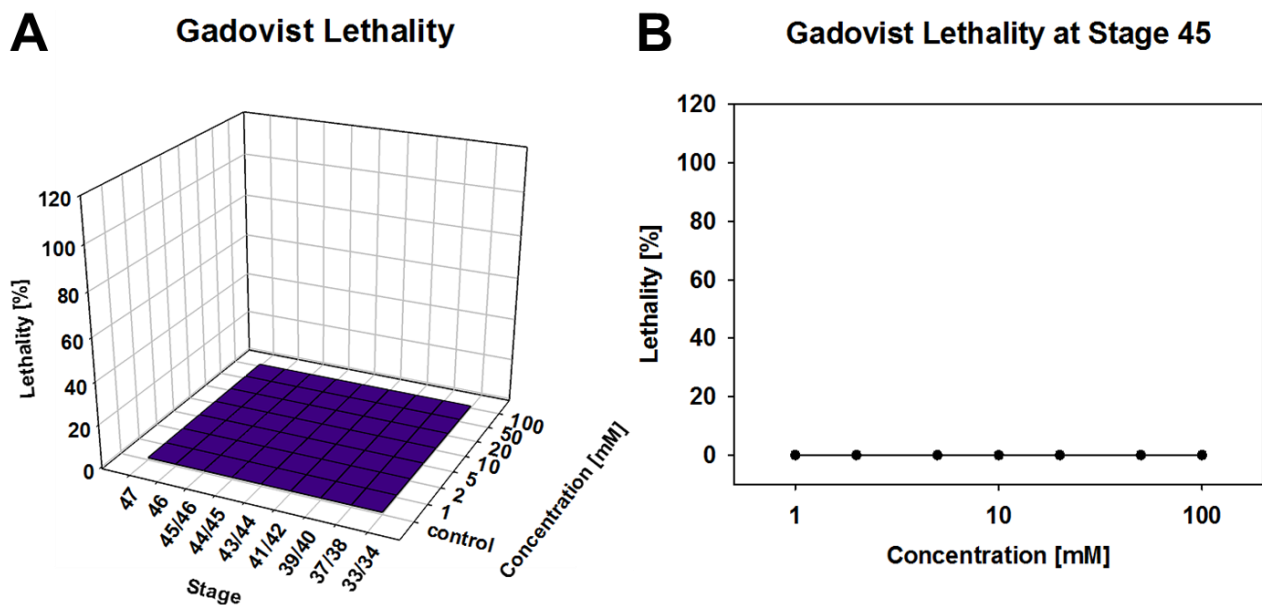

Fig. 23. Absence of lethality in Xenopus embryos treated with Gadovist. A: 3D-Mesh-Plot of embryonic lethality, stage, and concentration (n=3) **B**: Line and scatter plot of observed embryonic lethality at stage 45.

Treatment of embryos with Magnograf, MultiHance, and Dotarem led to dose- and incubation time-dependent lethality as documented in Fig. 24 to 26. All embryos treated with 100 mM Magnograf or MultiHance died within 24 hours, by when they had reached stage 37/38 (Fig. 24 and Fig. 25). At 50 mM, MultiHance was more lethal than Magnograf. The estimated LC_{50} values for Magnograf and MultiHance were 95.5 mM and 49.7 mM, respectively.
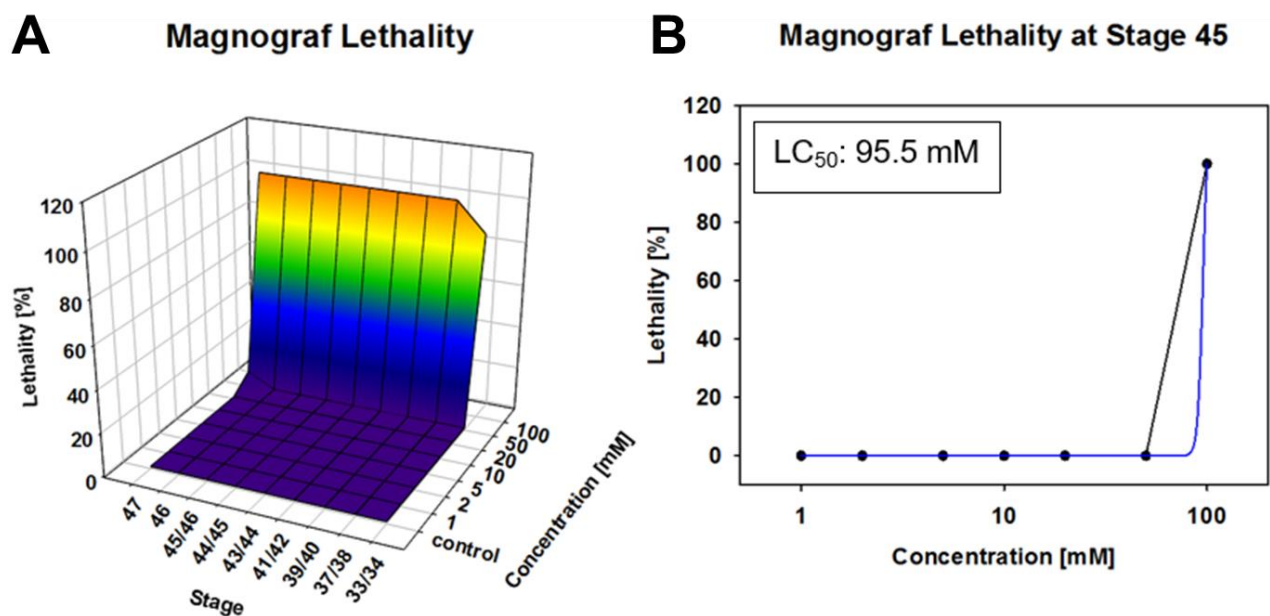

Fig. 24. Lethality of *Xenopus* embryos caused by Magnograf treatment. A: 3D-Mesh-Plot of embryonic lethality, stage, and concentration (*n*=3) **B**: Line and scatter plot of lethality at stage 45 for LC_{50} calculation. Standard deviation was 0.
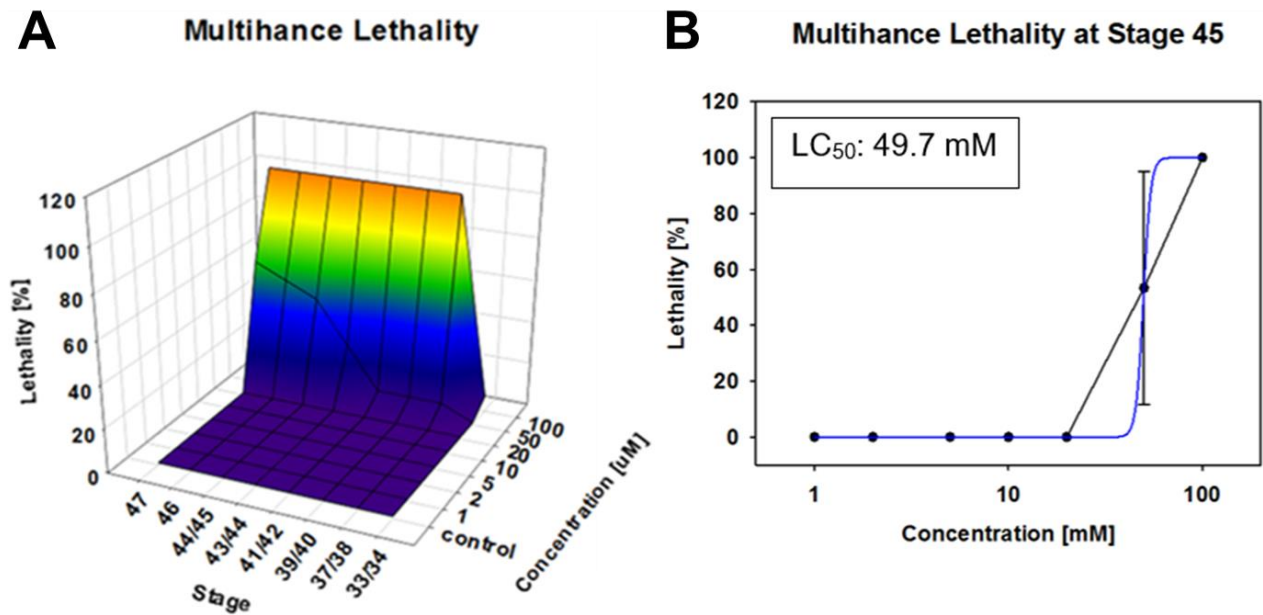
Fig. 25. Lethality of *Xenopus* embryos caused by MultiHance treatment. A: 3D-Mesh-Plot of embryonic lethality, stage, and concentration **B**: Line and scatter plot of lethality at stage 45 for LC_{50} calculation. Error bars indicate standard deviation.

Finally, embryos treated with Dotarem also showed dose- and incubation time-dependent lethality. However, lethality occurred later and approximately half of the embryos treated with 100 mM of Dotarem survived until the end of the experiment. The LC_{50} value were estimated to be about 107 mM (Fig. 26). A summary of the estimated EC_{50} values for hair cells toxicity and the LC_{50} values are shown in Table 9.

A Dotarem Lethality

B Dotarem Lethality at Stage 45

LC$_{50}$: 107 mM
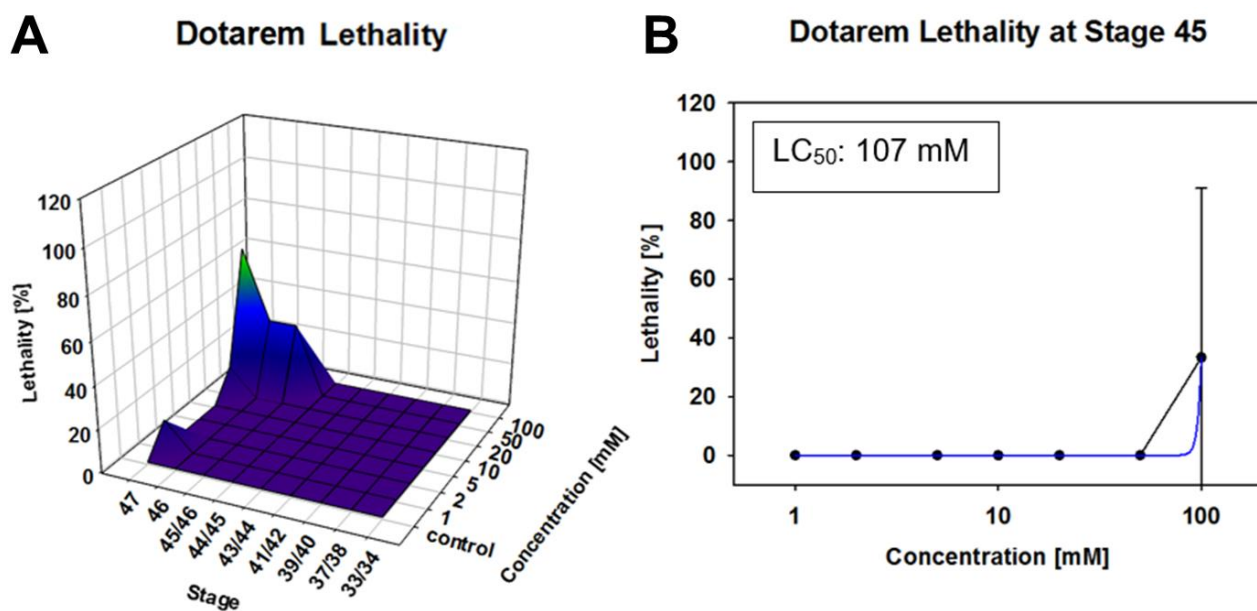
Fig. 26. Lethality of *Xenopus* embryos caused by Dotarem treatment. A: 3D-Mesh-Plot of embryonic lethality, stage, and concentration (*n*=3) **B**: Line and scatter plot of lethality at stage 45 for LC$_{50}$ calculation. Error bars indicate standard deviation.

Table 9. Compilation of the estimated EC$_{50}$ and LC$_{50}$ values for lateral line hair cell toxicity and lethality, respectively, after compound treatment

Compound	Ionicity	Structure	EC$_{50}$	LC$_{50}$
Gentamicin	n.a.	n.a.	2.0 µM	n.d.
Gadolinium trichloride	n.a.	n.a.	9.7 µM	56.7 µM
Omniscan	Non-ionic	Linear	a	b
Magnograf	Ionic	Linear	a	95.5 mM
MultiHance	Ionic	Linear	a	49.7 mM
Dotarem	Ionic	Macrocyclic	a	107 mM
Gadovist	Non-ionic	Macrocyclic	a	b

Abbreviations: a, hair cell toxicity too low for the calculation of EC$_{50}$ values; b, no embryonic lethality was observed; n.a., not applicable; n.d., not determined.

5 DISCUSSION

GBCAs are routinely used for MRI, where they are typically applied intravenously and excretion occurs via the kidney. In recent years, intratympanic GBCA injection followed by enhanced inner ear MRI has become a key diagnostic procedure in the diagnosis of Meniere´s disease. Gadolinium (Gd^{3+}), the main constituent of GBCAs, is highly toxic in its free form because of its similarities to Ca^{2+}, which is an important electrolyte required for heart and skeletal muscle contraction and nerve transmission. To harness the paramagnetic properties of Gd^{3+} for MRI purposes, the cation has to be chelated with polyaminopolycarboxylic acid that serves as ligand. Unstable chelates are considered unsafe for human use, as they could release free Gd^{3+}. A better understanding of the biodistribution and safety of GBCAs is therefore of high priority in order to address the serious safety concerns of these agents. In the present study, the lateral line system of *Xenopus* embryos was used as a fast, reproducible, and cost-effective *in vivo* test system to assess the hair cell toxicity potential of five commonly used GBCA that represent the main classes of GBCAs. The compounds were tested as concentrations similar to those used in humans. In addition, the concentrations lethal for *Xenopus* embryogenesis were established. Overall, the present work represents the first comparative *in vivo* toxicity assessment of multiple GBCAs in a vertebrate animal model.

5.1 *Xenopus* embryos are a Valid and Reliable Vertebrate Model Organism for Hair Cell Toxicity Testing

The lateral line of *Xenopus* embryos and tadpoles represents an ectodermal sensory organ consisting of mechanosensitive hair cells that detect water movements. Given its location in the skin, its hair cells are accessible to any drug or agent that presented in the media. This is a significant advantage over mammalian test systems that require oral or intravenous administration of compounds to assess their ototoxicity potential. After induction of ovulation, a single *Xenopus* female will give rise to hundreds of embryos,

which can be employed for extensive and comprehensive compound testing studies. Agents can be assessed *in vivo* over a wide concentration range to document hair cell toxicity. The hair cells of the lateral line can be selectively stained in batch with the fluorescent dye FM1-34FX. The dye is fixable and staining is confined to the lateral line's hair cells, if administered in the media to intact embryos (S. Schmitt *et al.*, manuscript in preparation). Compound-induced damage to lateral line hair cells will manifest in reduced fluorescent staining, which can be assessed by fluorescence stereomicroscopy. Quantitation of the remaining fluorescence after compound treatment serves as a basis to establish dose-response relationships and calculate of EC_{50} values. In addition, the treatment of the whole organism allows for the detection of compound-induced side effects and/or lethality. In the present study, each compound was assessed with at least 120 embryos for hair cell toxicity and typically a further 120 were used to characterize any possible adverse effects. Using a 48-well microplate set-up, the compound testing experiments could be performed efficiently and in a standard manner by harboring the embryos in home-made baskets. Embryos were moved from well to well to carry out the treatment, washing and staining steps with minimal transfer of medium.

By limiting the analysis of the fluorescent staining of the hair cells to the dorsolateral portions of the lateral line, natural variations from embryo to embryo could be addressed and imaging of the fluorescent hair cells was facilitated. Typically, control and treated embryos for each experimental set were derived from the same mating. Finally, the aminoglycoside gentamicin, a well-known ototoxic drug, was used to determine the effective concentration reducing fluorescent staining by half (EC_{50}). The obtained EC_{50} of 2.01 µM for gentamicin was very similar to the previously determined EC_{50} of 1.01 µM in our laboratory (S. Schmitt *et al.*, manuscript in preparation). This demonstrates that the *Xenopus*-based hair cell toxicity test system is robust and reproducible in the hands of different investigators.

5.2. Closer   Evolutionary   Relationship   Between Humans and *Xenopus* than Zebrafish

The lateral line of zebrafish larvae has been prominently used for large-scale *in vivo* hair cell toxicity screening purposes (Chiu et al., 2008). However, the toxicity of GBCAs has not been assessed in zebrafish to date. The zebrafish and *Xenopus* model systems share many experimental advantages, such the small sizes of the embryos, access to hundreds of embryos, and the presence of a lateral line system. With *Xenopus* ovulation and egg laying can be initiated at any time by hCG injection. Furthermore, frogs share an evolutionary history with mammals that is 90–100 million years longer than fish. It is therefore not surprising that the degree of morphological and functional similarities to humans is higher with *Xenopus* than zebrafish (Wheeler and Brandli, 2009).

5.3 Large   Scale   Dose-Response   Experiments   are Feasible with *Xenopus* Embryos

Guinea pigs and rats represent standard animal models for ototoxicity testing (Lataye et al., 2003; Poirrier et al., 2010). Testing is however restricted to the hair cells of the inner ear as mammals lack lateral line organs. Testing of water-borne compounds using hair cells of the lateral line offers the advantage that the compounds can administered and exposed at clearly defined concentrations with minimal interference by ADME (absorption, distribution, metabolism, and excretion) in mammalian *in vivo* models. Besides simple drug administration, moderate compound quantity requirements, low animal husbandry costs, and a simplified regulatory procedure are further advantages in favor of using *Xenopus* embryos for hair cell toxicity testing in comparison to rodents. However, rodents are evolutionary closer to humans and *Xenopus* lateral line hair cells may differ from inner ear hair cells in their sensitivity to toxic insults. Furthermore, *Xenopus* hair cell toxicity experiments are performed with embryos, thus the observed effects could have been influenced by developmental plasticity. The most compelling advantage of employing *Xenopus* embryos for drug toxicity testing is the possibility to

perform experiments that require large animal numbers, such as dose-response or comparative studies, as demonstrated in the present work.

5.4. *Xenopus* as a Useful Test System to Estimate the Risks of GBCA Enhanced Inner Ear MRI

The key advantage of GBCA enhanced inner ear MRI, as it is used for the visualization of ELH in Meniere´s and other diseases, is its ability to discriminate peri- and endolymphatic spaces by a selective GBCA enhancement in the perilymph, but not in the endolymph. The uptake of intratympanically administered GBCAs in the perilymph is very limited. After an intratympanic application of eight-fold diluted GBCA, the concentration in the perilymph is only 0.1 mM, which represents a 5000-fold dilution (Pyykko et al., 2010). High resolution images of strong field (9.4 T) MRI in mice could not detect a GBCA-increased signal intensity in the endolymph, when applied intravenously (Counter et al., 2013). In the present work, we studied GBCAs at concentrations from 1 to 100 mM. Hence, GBCAs toxicity testing in *Xenopus* was done at concentrations at and above the clinically applied concentration in patients, as well as the estimated concentration in the endolymph. Rupture of the Reissner´s membrane or morphological variations could lead to a considerable increase of GBCA concentrations in the endolymph. These special situations are adequately represented by the concentration ranges used in the present study. GBCA exposure time was 24 hours for *Xenopus* embryos. When performing inner ear MRI, the GBCA elimination half-life from perilymph was 6.6 hours for intratympanic and 3.2 hours for intravenous administration in guinea pigs (Li et al., 2013). This suggests that the treatment period used with *Xenopus* embryos was sufficiently similar. Previous studies have suggested, that the ototoxicity of intratympanically injected GBCAs could be caused by effects in other targets than hair cells (Kakigi et al., 2008; Nonoyama et al., 2016). It is likely that these aspects of GBCA toxicity cannot be captured in the *Xenopus* lateral line assay. Nevertheless, the assessment of GBCA toxicity for hair cells, which represents the key sensory organs of the inner ear, remains of primary concern.

5.5. Assessment of GBCA-induced Hair Cell Toxicity in *Xenopus*

Five common extracellular fluid GBCAs, approved for human application by the EMA and the FDA, were assessed for hair cell toxicity using the *Xenopus* lateral line. The selected GBCAs differ in the molecular structure of their chelates and the associated ionic properties. The examples cover all four GBCA types based on ligand structure (linear and macrocyclic) and ionicity (ionic or non-ionic). In general, the stability of the chelation of gadolinium to the ligand determines the safety of GBCAs. Non-ionic linear chelates are considered the least stable, while the ionic macrocyclic chelates are the most stable (Dekkers et al., 2018; Sherry et al., 2009). The toxicity of free gadolinium and the aminoglycoside gentamicin for hair cells of the mammalian inner ear is well established. In the present study, we demonstrate these two ototoxic compounds also damage hair cells of the lateral line of *Xenopus* embryos. With EC_{50} values of 2.0 µM and 9.7 µM for gentamicin and gadolinium trichloride, respectively, both compounds were toxic in the low µM range. These findings provide further validation for the use of the *Xenopus* lateral line system to assess ototoxicity. Unlike free gadolinium, none of the GBCAs induced considerable lateral line hair cell toxicity and hence no EC_{50} values could be established for the five GBCAs tested. Notably, the highest test concentration of 100 mM was 10'000-fold above the EC_{50} value of 9.7 µM for gadolinium-induced hair cell toxicity. While GBCA toxicity to hair cells of the lateral line was very limited, Magnograf and Dotarem causes a reduction in fluorescent dye labeling that was statistically significant. While both of these GBCA belong to the ionic class, which is associated with higher osmolality and toxic active ions, they differ in the structure of the ligand. Magnograf consists of a linear ligand, whereas Dotarem has a macrocyclic one. MultiHance, the third GBCA of the ionic class tested here, also showed reduction of fluorescent hair cells staining, which was however not statistically significant. Of all the GBCAs tested, Omniscan (based on a non-ionic linear chelator) and Gadovist (non-ionic macrocyclic) appear to be the least toxic for *Xenopus* lateral line hair cells.

5.6 GBCA-induced Hair Cell Toxicities Correlate across Animal Species

How do the findings on GBCA hair cell toxicities in *Xenopus* embryos compare to studies using other animal models? To date, no other animal model study than the present one has systematically investigated the hair cell toxicities of five different GBCAs in a comparative and standardized manner. Furthermore, cross-species comparison of GBCA toxicities has been difficult partly due to differing test methodologies. For Magnograf, studies in guinea pigs and human patients suggest that intratympanic application of an eight-fold dilution (62.5 mM) of the agent was non-toxic (Louza et al., 2015; Suzuki et al., 2011). However, the estimated GBCA concentration in the perilymph after intratympanic administration is only about 0.1 mM (Pyykko et al., 2010), and furthermore there is no evidence for permeation of the agent into endolymph and access to hair cells (Counter et al., 2013). Under the test conditions with *Xenopus* embryos, the hair cells of the lateral line are exposed directly to the GBCAs. The finding that Magnograf treatment causes moderate loss of fluorescent staining of lateral line hair cells at 10 mM and above may indicate that there is an inherent ototoxicity of Magnograf, which is only becomes apparent when hair cells are exposed directly to the agent.

The most widely studied GBCA regarding hair cell toxicity is Omniscan. In present study, no evidence for hair cell toxicity of Omniscan was observed for *Xenopus* lateral line hair cells, even at the highest concentration of 100 mM studied. In guinea pigs, Omniscan treatment similarly failed to not evoke physiological or morphological damage to hair cells at concentrations up to 500 mM (Duan et al., 2004; Suzuki et al., 2011; Zou et al., 2009). By contrast, Omniscan treatment of isolated bullfrog inner ear hair cells using four- to 16-fold dilutions of the agent (125 mM to 31.25 mM) caused significant toxicity (Tanaka et al., 2010). In mice, intratympanic administration of Omniscan caused mild ototoxicity as demonstrated by a significant change in auditory brainstem response (Nonoyama et al., 2016). Interestingly, the authors suggest that Omniscan may cause ototoxicity by a mechanism that does not involve outer hair cells, since these were found to be morphologically intact. Using in guinea pigs, Kakigi *et al.* (2008) reported toxic

effects to the stria vascularis and the endocochlear potential after intratympanic administration of Omniscan at concentrations over 32 mM (Kakigi et al., 2008). Importantly, no incidences of ototoxicity have been reported to date after intratympanic administration of eight-fold diluted Omniscan in humans (Louza et al., 2013). The absence of lateral line hair cell toxicity after treatment of *Xenopus* embryos with Omniscan is therefore consistent with the apparent lack of ototoxicity after intratympanic application of Omniscan in human patients.

5.6. Toxicity of GBCAs for *Xenopus* Embryos can be Attributed to Ionicity

While performing hair cell toxicity testing, we observed that the treatment with Magnograf or MultiHance at 100 mM (but not 50 mM) was lethal for the embryos within 24 hours. Interestingly, both agents are examples of GBCAs based on ionic linear chelates. To assess adverse side effects and systemic toxicity of GBCAs in greater detail, *Xenopus* embryos were treated with the agents at concentrations ranging from 1 mM to 100 mM and the embryos were observed over a treatment period of five days for evidence of GBCA-induced lethality. Free gadolinium, which was toxic with an LC_{50} of 56.7 µM, was used as a benchmark. None of the GBCAs tested were toxic at concentrations up to 20 mM. Beyond this concentration, significant differences in lethality were observed between the different GBCAs tested. While Omniscan and Gadovist caused no lethality even at 100 mM, Magnograf, MultiHance, and Dotarem treatment led to a dose- and incubation time-dependent increase of embryonic lethality with estimated LC_{50} values ranging from 49.7 to 107 mM. The nonlethal Omniscan and Gadovist represent non-ionic GBCAs with linear and macrocyclic ligand structures, respectively. By contrast, ionic GBCAs caused lethality at concentrations of 50 mM or higher irrespective of the ligand structure. It therefore appears that ionicity (and not ligand structure) represents the key physicochemical determinant for the lethality of GBCAs in *Xenopus* embryos. Ionic GBCAs harbor counterions bound via ionic bonds to the ligand that dissociate in water and increase the osmolality. The presence of counterions can therefore contribute to the toxicity of GBCAs (Kun and Jakubowski,

2012). The skin of aquatic fish and amphibian larvae is primarily permeable to small, hydrophobic organic molecules with logP values higher than +1 (Wheeler and Brandli, 2009). As summarized in in Table 3, all GBCAs tested in the present study have logP values ranging between -3.16 and -2.0. Given their hydrophilicity, it is unlikely that GBCAs are absorbed by *Xenopus* embryos. In addition, the ionic GBCAs had higher molecular masses (754-1058 g/mol) than the non-toxic, non-ionic GBCAs (592-605 g/mol), which correlates negatively with compound absorption. Finally, active ingestion of GBCAs by *Xenopus* embryos can be excluded as food uptake starts after stage 45, the endpoint used to determine compound-induced lethality. It is therefore most likely that the lethal effects of ionic GBCAs on *Xenopus* embryogenesis can be attributed to the increase in osmolality in the culture media, which is caused by the massive release of counterions at high GBCA concentrations.

5.7 Comparison of GBCA Toxicities across Animal Species

The toxicity and lethal doses of GBCAs for mammals have been established primarily for rats in various studies (see Table 10 for references). A direct comparison of the quantitative data for a given GBCA between *Xenopus* and mammalian test systems is however difficult due differences in administration mode, testing situation (*in vivo* vs. *in vitro*) and age of the individuals used for testing. We therefore compared the rank orders of reported toxicities (Table 10). Interestingly, the low toxicity of the non-ionic GBCAs Omniscan and Gadovist correlated well with results obtained from studies in rats and human blood. For example, lethality testing of GBCAs in rats by intravenous administration of GBCAs in rat demonstrated that Omniscan and Gadovist were significantly less toxic than the other GBCAs. As for *Xenopus* embryos, acute lethality of GBCAs in rats correlates well with the iconicity, where ionic GBCAs exhibit higher toxicity than non-ionic ones irrespective of the ligand structure. Chelate stability, *i.e.* release of gadolinium, appears therefore to be less of factor for acute lethality than ionic imbalances cause by counterion release by ionic GBCAs. A different perspective is provided by the risk ranking of GBCAs for nephrogenic systemic fibrosis (NSF) (EMA,

2010). The fibrosis risk is determined in part by gadolinium release from the chelate and the tissue retention of GBCAs. Macrocyclic GBCAs are considered to have a lower fibrosis risk than linear ones. Hence, Dotarem scores low, while Omniscan's risk is high (Table 10).

Table 10: Comparison of GBCA toxicity rank orders across animal models

Toxicity	high ⟶			low
***Xenopus* embryos** External administration (LC_{50}, mM)	MultiHance (49.7)	Magnograf (95.5)	Dotarem (107)	Omniscan (ND) Gadovist (ND)
Rat i.v. administration (LD_{50}, mmol/kg) (Oksendal and Hals, 1993), (Gries, 2002)	Magnograf (8)	MultiHance (10)	Dotarem (18)	Omniscan (25) Gadovist (25)
Human blood *In vitro* (Gd-release in %) (Frenzel et al., 2008)	Omniscan (20)	Magnograf (1.9) MultiHance (1.9)		Dotarem (< 0.1) Gadovist (< 0.1)
Rat i.v. administration (Gd-release in µM Gd/g skin) (Sieber et al., 2008)	Omniscan (~ 1.7)	Magnograf (~ 0.2) MultiHance (~ 0.1)		Dotarem (~ 0.05) Gadovist (~ 0.05)
Risk for nephrogenic systemic fibrosis (EMA, 2010)	Omniscan (high) Magnograf (high)	MultiHance (medium)		Dotarem (low) Gadovist (low)

Examples of toxicity rank orders as determined in the present study and the cited references.

6 CONCLUSIONS AND PERSPECTIVES

The issues concerning the toxicity of GBCAs have been gaining extensive attention in recent years. In 2007, the development of nephrogenic systemic fibrosis in patients with severe renal insufficiency was linked to exposure of high doses of gadolinium (Daftari Besheli et al., 2014; Perazella, 2009). More recently, gadolinium deposition after i.v. administration in healthy individuals was confirmed challenging the safety of GBCAs (Kanda et al., 2015; Kanda et al., 2017; McDonald et al., 2017; Ramalho et al., 2016). Finally, in 2017 the EMA recommended to suspend the use of four GBCAs of the linear ligand class, mainly due to the higher risk of retention and accumulation in the human body (Dekkers et al., 2018). Importantly, the suspended linear GBCAs are of both the ionic and non-ionic type. The use of a further linear GBCA, MultiHance, was restricted, whereas maintenance was only recommended for Primovist as the only linear GBCA left. In the present study, the hair cell toxicities and potentially lethal effects of five GBCAs were examined using *Xenopus* embryos. Among the tested GBCAs in *Xenopus*, Magnograf and Omniscan are now recommended for suspension and Multihance is under restriction by the EMA. Only the macrocyclic Dotarem and Gadovist are considered GBCA safe for use in humans.

How well does toxicity testing of GBCAs in *Xenopus* embryos predict their effects in human patients? Regarding potential ototoxicity, the lateral line hair cell toxicity tests in *Xenopus* embryos failed to reveal overt toxicity of any of the tested agents. While mild and statistically significant hair cell damage was detected with two ionic GBCAs (Magnograf, Dotarem), in no case was it possible to calculate EC_{50} values. For all assessed GBCAs, hair cell toxicity was evidently absent or low at concentrations used clinically for intratympanic administrations. Overall, hair cell toxicity testing in *Xenopus* provides further supportive evidence for the safe use of GBCAs in MR imaging to study inner ear defects, such the visualization of EH. The importance of stable binding of gadolinium to its ligand was underscored by the potent toxicity of free gadolinium (EC_{50}: 9.7 µM) towards the hair cells of the lateral line. Concerns for general toxicity of GBCAs arose from the observation that 24-hour incubation of *Xenopus* embryos with 100 mM of Magnograf or MultiHance resulted in embryonic lethality. Long-term treatment of

Xenopus embryos with water-borne GBCAs revealed that all GBCAs of the ionic type irrespective of the ligand structure caused embryonic lethality at concentrations above 50 mM. By contrast, none of the non-ionic GBCAs tested were lethal for *Xenopus* embryos. The general toxicities of GBCAs observed in *Xenopus* embryos were in line with previous observation from testing in rats. It should be noted that the *Xenopus* toxicity tests do not predict the long-term effects of GBCAs in the vertebrate body, such as damages caused by gadolinium retention in the brain and other organs. In fact, it is very likely that there is no uptake of GBCAs at all into *Xenopus* embryos as the animals do not feed yet and the agents are too hydrophilic to be absorbed via the epidermis.

Overall, the present work establishes *Xenopus* embryos as a valid, reliable, and objective test system to assess and quantitate the hair cell toxicity of any water-borne GBCA. Given the virtually unlimited access to *Xenopus* embryos, large-scale testing of GBCAs for comparative purposes is now feasible. In our opinion, *Xenopus* hair cell toxicity testing may in future replace expensive and laborious testing in mammals as initial, *in vivo* whole organism test system for novel experimental GBCAs. In this context, only those GBCAs scoring as non-toxic in *Xenopus* embryos would be advanced for testing in mammalian animal models. The recently updated recommendations of the EMA for the use of GBCAs in humans (Dekkers et al. 2018) include five agents that were not yet assessed in *Xenopus* embryos. These include Primovist (gadoxenate), the only linear GBCA left on the recommendation list, and the linear Optimark (gadoversetamide) and macrocyclic Prohance (gadoteridol) that could be assessed in *Xenopus* for hair cell toxicities.

The most practical conclusions that can be drawn from the *Xenopus* GBCA toxicity studies reported here and the recent recommendation by the EMA on the use of GBCAs (Dekkers et al. 2018) are as follows. First, Gadovist and Omniscan have emerged as those GBCAs causing the least damage to *Xenopus* lateral line hair cells. Second, Gadovist and Omniscan, both representing GBCAs of the non-ionic type, appear to have favorable safety profiles given that they do not cause any lethality in *Xenopus* embryos. Finally, the recent safety recommendation by the EMA suspends the use of Omniscan. Taken together, this favors the use of the non-ionic macrocyclic Gadovist for intratympanic enhanced MRI.

7 REFERENCES

Aime, S., and Caravan, P. (2009). Biodistribution of gadolinium-based contrast agents, including gadolinium deposition. J Magn Reson Imaging *30*, 1259-1267.

Akgun, H., Gonlusen, G., Cartwright, J., Jr., Suki, W.N., and Truong, L.D. (2006). Are gadolinium-based contrast media nephrotoxic? A renal biopsy study. Arch Pathol Lab Med *130*, 1354-1357.

Alexander, T.H., and Harris, J.P. (2010). Current epidemiology of Meniere's syndrome. Otolaryngol Clin North Am *43*, 965-970.

Andrade Yé, N., Fernandes, J., Vázquez, E., Fernández-Fernández Jé, M., Arniges, M., Sánchez, T.M., Villalón, M., and Valverde, M.A. (2005). TRPV4 channel is involved in the coupling of fluid viscosity changes to epithelial ciliary activity. J Cell Biol *168*, 869-874.

Appel, G.B., and Neu, H.C. (1978). Gentamicin in 1978. Ann Intern Med *89*, 528-538.

Baker, C.V.H. (2008). Lateral line, otic and epibranchial placodes: developmental and evolutionary links? J Exp Zool B Mol Dev Evol. *310*, 370-383.

Baloh, R.W. (2001). Prosper ménière and his disease. Arch Neurol *58*, 1151-1156.

Bellin, M.F., and Van Der Molen, A.J. (2008). Extracellular gadolinium-based contrast media: an overview. Eur J Radiol *66*, 160-167.

Bennett, C.L., Qureshi, Z.P., Sartor, A.O., Norris, L.A.B., Murday, A., Xirasagar, S., and Thomsen, H.S. (2012). Gadolinium-induced nephrogenic systemic fibrosis: the rise and fall of an iatrogenic disease. Clin Kidney J *5*, 82-88.

Blasco-Perrin, H., Glaser, B., Pienkowski, M., Peron, J.M., and Payen, J.L. (2013). Gadolinium induced recurrent acute pancreatitis. Pancreatology *13*, 88-89.

Bley, C.-H., Centgraf, M., Cieslik, A., Hack, J., and Hohloch, L. (2015). I care Anatomie, Physiologie, 1 edn (Thieme).

Brownell, W., Bader, C., Bertrand, D., and de Ribaupierre, Y. (1985). Evoked mechanical responses of isolated cochlear outer hair cells. Science (New York, NY) *227*, 194-196.

Bykowski, J., Harris, J.P., Miller, M., Du, J., and Mafee, M.F. (2015). Intratympanic Contrast in the Evaluation of Menière Disease: Understanding the Limits. Am J Neuroradiol *36*, 1326-1332.

Chen, C., Chen, Y., Wu, P., and Chen, B. (2014). Update on new medicinal applications of gentamicin: evidence-based review. J Formos Med Assoc *113*, 72-82.

Chen, R., Ling, D., Zhao, L., Wang, S., Liu, Y., Bai, R., Baik, S., Zhao, Y., Chen, C., and Hyeon, T. (2015). Parallel Comparative Studies on Mouse Toxicity of Oxide Nanoparticle- and Gadolinium-Based T1 MRI Contrast Agents. ACS nano *9*, 12425-12435.

Cheong, B.Y.C., and Muthupillai, R. (2010). Nephrogenic Systemic Fibrosis: A Concise Review for Cardiologists. Tex Heart Inst J *37*, 508-515.

Chiu, L.L., Cunningham, L.L., Raible, D.W., Rubel, E.W., and Ou, H.C. (2008). Using the Zebrafish Lateral Line to Screen for Ototoxicity. J Assoc Res Otolaryngol *9*, 178-190.

Cochilla, A.J., Angleson, J.K., and Betz, W.J. (1999). Monitoring secretory membrane with FM1-43 fluorescence. Annu Rev Neurosci *22*, 1-10.

Coombs, S., Bleckmann, H., Fay, R.R., and Popper, A.N. (2013). The Lateral Line System (Heidelberg: Springer Verlag Berlin).

Counter, S.A., Bjelke, B., Borg, E., Klason, T., Chen, Z., and Duan, M.L. (2000). Magnetic resonance imaging of the membranous labyrinth during in vivo gadolinium (Gd-DTPA-BMA) uptake in the normal and lesioned cochlea. Neuroreport *11*, 3979-3983.

Counter, S.A., Nikkhou, S., Brené, S., Damberg, P., Sierakowiak, A., Klason, T., Berglin, C., and Laurell, G. (2013). MRI Evidence of Endolymphatic Impermeability to the Gadolinium Molecule in the In Vivo Mouse Inner Ear at 9.4 Tesla. Open Neuroimag J *7*, 27-31.

Daftari Besheli, L., Aran, S., Shaqdan, K., Kay, J., and Abujudeh, H. (2014). Current status of nephrogenic systemic fibrosis. Clin Radiol *69*, 661-668.

Dekkers, I.A., Roos, R., and van der Molen, A.J. (2018). Gadolinium retention after administration of contrast agents based on linear chelators and the recommendations of the European Medicines Agency. Eur Radiol *28*, 1579-1584.

Duan, M., Bjelke, B., Fridberger, A., Counter, S.A., Klason, T., Skjonsberg, A., Herrlin, P., Borg, E., and Laurell, G. (2004). Imaging of the guinea pig cochlea following round window gadolinium application. Neuroreport *15*, 1927-1930.

Eckhard, A., Müller, M., Salt, A., Smolders, J., Rask-Andersen, H., and Löwenheim, H. (2014). Water permeability of the mammalian cochlea: functional features of an aquaporin-facilitated water shunt at the perilymph–endolymph barrier. Pflugers Arch *466*, 1963-1985.

Elmstahl, B., Nyman, U., Leander, P., Chai, C.M., Golman, K., Bjork, J., and Almen, T. (2006). Gadolinium contrast media are more nephrotoxic than iodine media. The importance of osmolality in direct renal artery injections. Eur Radiol *16*, 2712-2720.

EMA (2010). Assessment report for Gadolinium-containing contrast agents. In Proced No EMEA/H/A-31/1097 (http://www.ema.europa.eu/docs/en_GB/document_library/Referrals_document/gadolinium_31/WC500099538.pdf).

Farris, H.E., LeBlanc, C.L., Goswami, J., and Ricci, A.J. (2004). Probing the pore of the auditory hair cell mechanotransducer channel in turtle. J Physiol *558*, 769-792.

FDA (2006). Public health advisory: Gadolinium-containing contrast agents for magnetic resonance imaging (MRI): Omniscan, OptiMark, Magnevist, ProHance, and MultiHance (http://www.fda.gov/cder/drug/advisory/gadolinium_agents.htm).

Fettiplace, R., and Kim, K.X. (2014). The Physiology of Mechanoelectrical Transduction Channels in Hearing. Physiol Rev *94*, 951-986.

Foster, C.A., and Breeze, R.E. (2013). Endolymphatic hydrops in Meniere's disease: cause, consequence, or epiphenomenon? Otol Neurotol *34*, 1210-1214.

Frenzel, T., Lengsfeld, P., Schirmer, H., Hutter, J., and Weinmann, H.J. (2008). Stability of gadolinium-based magnetic resonance imaging contrast agents in human serum at 37 degrees C. Invest Radiol *43*, 817-828.

Gale, J.E., Marcotti, W., Kennedy, H.J., Kros, C.J., and Richardson, G.P. (2001). FM1-43 dye behaves as a permeant blocker of the hair-cell mechanotransducer channel. J Neurosci *21*, 7013-7025.

Goycoolea, M.V., and Lundman, L. (1997). Round window membrane. Structure function and permeability: a review. Microsc Res Tech *36*, 201-211.

Gries, H. (2002). Extracellular MRI Contrast Agents Based on Gadolinium. In Contrast Agents I: Magnetic Resonance Imaging, W. Krause, ed. 1 (Berlin, Heidelberg: Springer Berlin Heidelberg), pp. 1-24.

Grobner, T. (2006). Gadolinium--a specific trigger for the development of nephrogenic fibrosing dermopathy and nephrogenic systemic fibrosis? Nephrol Dial Transplant *21*, 1104-1108.

Gurkov, R., Flatz, W., Louza, J., Strupp, M., Ertl-Wagner, B., and Krause, E. (2012). In vivo visualized endolymphatic hydrops and inner ear functions in patients with electrocochleographically confirmed Meniere's disease. Otol Neurotol *33*, 1040-1045.

Gurkov, R., and Hornibrook, J. (2018). On the classification of hydropic ear disease (Meniere's disease). Hno.

Gurkov, R., Kantner, C., Strupp, M., Flatz, W., Krause, E., and Ertl-Wagner, B. (2014). Endolymphatic hydrops in patients with vestibular migraine and auditory symptoms. Eur Arch Otorhinolaryngol *271*, 2661-2667.

Gurkov, R., Pyyko, I., Zou, J., and Kentala, E. (2016). What is Meniere's disease? A contemporary re-evaluation of endolymphatic hydrops. J Neurol *263 Suppl 1*, S71-81.

Gurkov, R., Pyykö, I., Zou, J., and Kentala, E. (2016). What is Menière's disease? A contemporary re-evaluation of endolymphatic hydrops. J Neurol *263*, 71-81.

Haley, T.J. (1965). Pharmacology and Toxicology of the Rare Earth Elements. J Pharm Sci *54*, 663-670.

Havia, M., Kentala, E., and Pyykko, I. (2005). Prevalence of Meniere's disease in general population of Southern Finland. Otolaryngol Head Neck Surg *133*, 762-768.

Heinrich, M.C., Kuhlmann, M.K., Kohlbacher, S., Scheer, M., Grgic, A., Heckmann, M.B., and Uder, M. (2007). Cytotoxicity of iodinated and gadolinium-based contrast agents in renal tubular cells at angiographic concentrations: in vitro study. Radiology *242*, 425-434.

Hirano, S., and Suzuki, K.T. (1996). Exposure, metabolism, and toxicity of rare earths and related compounds. Environ Health Perspect *104*, 85-95.

Hobson, B.M. (1958). Some observations on the use of female Xenopus laevis for the diagnosis of pregnancy. Am J Obstet Gynecol *75*, 825-828.

Hsieh, L.-C., Lin, H.-C., Tsai, H.-T., Ko, Y.-C., Shu, M.-T., and Lin, L.-H. (2009). High-dose intratympanic gentamicin instillations for treatment of Meniere's disease: long-term results. Acta Otolaryngol *129*, 1420-1424.

Hui, F.K., and Mullins, M. (2009). Persistence of gadolinium contrast enhancement in CSF: a possible harbinger of gadolinium neurotoxicity? AJNR Am J Neuroradiol *30*, E1.

Idée, J.-M., Fretellier, N., Robic, C., and Corot, C. (2014). The role of gadolinium chelates in the mechanism of nephrogenic systemic fibrosis: A critical update. Crit Rev Toxicol *44*, 895-913.

Iida, T., Teranishi, M., Yoshida, T., Otake, H., Sone, M., Kato, M., Shimono, M., Yamazaki, M., Naganawa, S., and Nakashima, T. (2013). Magnetic resonance imaging of the inner ear after both intratympanic and intravenous gadolinium injections. Acta Otolaryngol *133*, 434-438.

Inamoto, R., Miyashita, T., Akiyama, K., Mori, T., and Mori, N. (2009). Endolymphatic sac is involved in the regulation of hydrostatic pressure of cochlear endolymph. Am J Physiol Regul Integr Comp Physiol *297*, R1610-1614.

James-Zorn, C., Ponferrada, V., Fisher, M.E., Burns, K., Fortriede, J., Segerdell, E., Karimi, K., Lotay, V., Wang, D.Z., Chu, S.*, et al.* (2018). Navigating Xenbase: An Integrated Xenopus

Genomics and Gene Expression Database. In Eukaryotic Genomic Databases: Methods and Protocols, M. Kollmar, ed. (New York, NY: Springer New York), pp. 251-305.

Kakigi, A., Nishimura, M., Takeda, T., Okada, T., Murata, Y., and Ogawa, Y. (2008). Effects of gadolinium injected into the middle ear on the stria vascularis. Acta Otolaryngol *128*, 841-845.

Kalmijn, A.J. (1989). Functional Evolution of Lateral Line and Inner Ear Sensory Systems. In The Mechanosensory Lateral Line: Neurobiology and Evolution, S. Coombs, P. Görner, and H. Münz, eds. (New York, NY: Springer New York), pp. 187-215.

Kanda, T., Fukusato, T., Matsuda, M., Toyoda, K., Oba, H., Kotoku, J., Haruyama, T., Kitajima, K., and Furui, S. (2015). Gadolinium-based Contrast Agent Accumulates in the Brain Even in Subjects without Severe Renal Dysfunction: Evaluation of Autopsy Brain Specimens with Inductively Coupled Plasma Mass Spectroscopy. Radiology *276*, 228-232.

Kanda, T., Nakai, Y., Hagiwara, A., Oba, H., Toyoda, K., and Furui, S. (2017). Distribution and chemical forms of gadolinium in the brain: a review. Br J Radiol *90*, 20170115.

Katahira, N., Tanigawa, T., Tanaka, H., Nonoyama, H., and Ueda, H. (2013). Diluted gadoteridol (ProHance(R)) causes mild ototoxicity in cochlear outer hair cells. Acta Otolaryngol *133*, 788-795.

Kellerhals, B. (1976). Quantitative assessment of perilymph sources. ORL J Otorhinolaryngol Relat Spec *38*, 193-197.

Kimitsuki, T., Nakagawa, T., Hisashi, K., Komune, S., and Komiyama, S. (1996). Gadolinium blocks mechano-electric transducer current in chick cochlear hair cells. Hear Res *101*, 75-80.

Kimura, R.S. (1967). Experimental blockage of the endolymphatic duct and sac and its effect on the inner ear of the guinea pig. A study on endolymphatic hydrops. Ann Otol Rhinol Laryngol *76*, 664-687.

Kraske, S., Cunningham, J.T., Hajduczok, G., Chapleau, M.W., Abboud, F.M., and Wachtel, R.E. (1998). Mechanosensitive ion channels in putative aortic baroreceptor neurons. Am J Physiol *275*, H1497-1501.

Kun, T., and Jakubowski, L. (2012). Influence of MRI contrast media on histamine release from mast cells. Pol J Radiol *77*, 19-24.

Lang, F., Vallon, V., Knipper, M., and Wangemann, P. (2007). Functional significance of channels and transporters expressed in the inner ear and kidney. Am J Physiol Cell Physiol *293*, C1187-1208.

Lataye, R., Campo, P., Pouyatos, B., Cossec, B., Blachere, V., and Morel, G. (2003). Solvent ototoxicity in the rat and guinea pig. Neurotoxicol Teratol *25*, 39-50.

Lewis, R.S., and Hudspeth, A.J. (1983). Voltage- and ion-dependent conductances in solitary vertebrate hair cells. Nature *304*, 538-541.

Li, J., Yu, L., Xia, R., Gao, F., Luo, W., and Jing, Y. (2013). Postauricular hypodermic injection to treat inner ear disorders: experimental feasibility study using magnetic resonance imaging and pharmacokinetic comparison. J Laryngol Otol *127*, 239-245.

Lopez-Escamez, J.A., Carey, J., Chung, W.H., Goebel, J.A., Magnusson, M., Mandala, M., Newman-Toker, D.E., Strupp, M., Suzuki, M., Trabalzini, F.*, et al.* (2015). Diagnostic criteria for Meniere's disease. J Vestib Res *25*, 1-7.

Louza, J., Krause, E., and Gurkov, R. (2013). Audiologic evaluation of Meniere's disease patients one day and one week after intratympanic application of gadolinium contrast agent: our experience in sixty-five patients. Clin Otolaryngol *38*, 262-266.

Louza, J., Krause, E., and Gurkov, R. (2015). Hearing function after intratympanic application of gadolinium-based contrast agent: A long-term evaluation. Laryngoscope *125*, 2366-2370.

Louza, J.P., Flatz, W., Krause, E., and Gurkov, R. (2012). Short-term audiologic effect of intratympanic gadolinium contrast agent application in patients with Meniere's disease. Am J Otolaryngol *33*, 533-537.

Lustig, L.R., and Lalwani, A. (1997). The history of Meniere's disease. Otolaryngol Clin North Am *30*, 917-945.

McDonald, R.J., McDonald, J.S., Kallmes, D.F., Jentoft, M.E., Paolini, M.A., Murray, D.L., Williamson, E.E., and Eckel, L.J. (2017). Gadolinium Deposition in Human Brain Tissues after Contrast-enhanced MR Imaging in Adult Patients without Intracranial Abnormalities. Radiology *285*, 546-554.

Merchant, S.N., Rauch, S.D., and Nadol, J.B., Jr. (1995). Meniere's disease. Eur Arch Otorhinolaryngol *252*, 63-75.

Meyers, J.R., MacDonald, R.B., Duggan, A., Lenzi, D., Standaert, D.G., Corwin, J.T., and Corey, D.P. (2003). Lighting up the senses: FM1-43 loading of sensory cells through nonselective ion channels. J Neurosci *23*, 4054-4065.

Minor, L.B., Schessel, D.A., and Carey, J.P. (2004). Meniere's disease. Curr Opin Neurol *17*, 9-16.

Monsell, E.M., Balkany, T.A., Gates, G.A., Goldenberg, R.A., Meyerhoff, W.L., and J.W., H. (1995). Committee on Hearing and Equilibrium Guidelines for the diagnosis and evaluation of therapy in Meniere's disease. Otolaryngol Head Neck Surg *113*, 181–185

Naganawa, S., and Nakashima, T. (2014). Visualization of endolymphatic hydrops with MR imaging in patients with Ménière's disease and related pathologies: current status of its methods and clinical significance. Jpn J Radiol *32*, 191-204.

Naganawa, S., Satake, H., Kawamura, M., Fukatsu, H., Sone, M., and Nakashima, T. (2008). Separate visualization of endolymphatic space, perilymphatic space and bone by a single pulse sequence; 3D-inversion recovery imaging utilizing real reconstruction after intratympanic Gd-DTPA administration at 3 Tesla. Eur Radiol *18*, 920-924.

Naganawa, S., Yamazaki, M., Kawai, H., Bokura, K., Iida, T., Sone, M., and Nakashima, T. (2014). MR imaging of Meniere's disease after combined intratympanic and intravenous injection of gadolinium using HYDROPS2. Magn Reson Med Sci *13*, 133-137.

Naganawa, S., Yamazaki, M., Kawai, H., Bokura, K., Sone, M., and Nakashima, T. (2012). Imaging of Meniere's disease after intravenous administration of single-dose gadodiamide: utility of subtraction images with different inversion time. Magn Reson Med Sci *11*, 213-219.

Nakashima, T., Naganawa, S., Sugiura, M., Teranishi, M., Sone, M., Hayashi, H., Nakata, S., Katayama, N., and Ishida, I.M. (2007). Visualization of endolymphatic hydrops in patients with Meniere's disease. Laryngoscope *117*, 415-420.

Nakashima, T., Naganawa, S., Teranishi, M., Tagaya, M., Nakata, S., Sone, M., Otake, H., Kato, K., Iwata, T., and Nishio, N. (2010). Endolymphatic hydrops revealed by intravenous gadolinium injection in patients with Ménière's disease. Acta Otolaryngol *130*, 338-343.

Nieuwkoop, P.D., and Faber, J. (1967). Normal Table of Xenopus laevis (Daudin) (Amsterdam: North-Holland Publishing Co.).

Nishikawa, S., and Sasaki, F. (1996). Internalization of styryl dye FM1-43 in the hair cells of lateral line organs in Xenopus larvae. J Histochem Cytochem *44*, 733-741.

Nonoyama, H., Tanigawa, T., Shibata, R., Tanaka, H., Katahira, N., Horibe, Y., Takemura, K., Murotani, K., Ozeki, N., and Ueda, H. (2016). Investigation of the ototoxicity of gadoteridol (ProHance) and gadodiamide (Omniscan) in mice. Acta Otolaryngol *136*, 1091-1096.

Oas, J.G., and Baloh, R.W. (1992). Vertigo and the anterior inferior cerebellar artery syndrome. Neurology *42*, 2274-2279.

Oksendal, A.N., and Hals, P.A. (1993). Biodistribution and toxicity of MR imaging contrast media. J Magn Reson Imaging *3*, 157-165.

Paulsen, F., and Waschke, J. (2010). Sobotta, Atlas der Anatomie des Menschen Band 3. In Kopf, Hals und Neuroanatomie (Urban & Fischer Verlag/Elsevier GmbH).

Perazella, M.A. (2009). Current status of gadolinium toxicity in patients with kidney disease. Clin J Am Soc Nephrol *4*, 461-469.

Perez-Rodriguez, J., Lai, S., Ehst, B.D., Fine, D.M., and Bluemke, D.A. (2009). Nephrogenic systemic fibrosis: incidence, associations, and effect of risk factor assessment--report of 33 cases. Radiology *250*, 371-377.

Plontke, S.K., and Gurkov, R. (2015). [Meniere's Disease]. Laryngorhinootologie *94*, 530-554.

Plontke, S.K., Wood, A.W., and Salt, A.N. (2002). Analysis of gentamicin kinetics in fluids of the inner ear with round window administration. Otol Neurotol *23*, 967-974.

Poirrier, A.L., Van den Ackerveken, P., Kim, T.S., Vandenbosch, R., Nguyen, L., Lefebvre, P.P., and Malgrange, B. (2010). Ototoxic drugs: difference in sensitivity between mice and guinea pigs. Toxicol Lett *193*, 41-49.

Port, M., Idee, J.M., Medina, C., Robic, C., Sabatou, M., and Corot, C. (2008). Efficiency, thermodynamic and kinetic stability of marketed gadolinium chelates and their possible clinical consequences: a critical review. Biometals *21*, 469-490.

Pullens, B., and van Benthem, P.P. (2011). Intratympanic gentamicin for Meniere's disease or syndrome. Cochrane Database Syst Rev CD008234

Purves, D., Augustine, G., and Fitzpatrick, D. (2001). Hair Cells and the Mechanoelectrical Transduction of Sound Waves, 2 edn (Sunderland (MA): Sinauer Associates).

Pyykko, I., Nakashima, T., Yoshida, T., Zou, J., and Naganawa, S. (2013). Meniere's disease: a reappraisal supported by a variable latency of symptoms and the MRI visualisation of endolymphatic hydrops. BMJ open *3*.

Pyykko, I., Zou, J., Poe, D., Nakashima, T., and Naganawa, S. (2010). Magnetic resonance imaging of the inner ear in Meniere's disease. Otolaryngol Clin North *43*, 1059-1080.

Ramalho, J., Semelka, R.C., Ramalho, M., Nunes, R.H., AlObaidy, M., and Castillo, M. (2016). Gadolinium-Based Contrast Agent Accumulation and Toxicity: An Update. AJNR Am J Neuroradiol *37*, 1192-1198.

Rask-Andersen, H., DeMott, J.E., Bagger-Sjoback, D., and Salt, A.N. (1999). Morphological changes of the endolymphatic sac induced by microinjection of artificial endolymph into the cochlea. Hear Res *138*, 81-90.

Rauch, S.D., Merchant, S.N., and Thedinger, B.A. (1989). Meniere's syndrome and endolymphatic hydrops. Double-blind temporal bone study. Ann Otol Rhinol Laryngol *98*, 873-883.

Ray, D.E., Cavanagh, J.B., Nolan, C.C., and Williams, S.C. (1996). Neurotoxic effects of gadopentetate dimeglumine: behavioral disturbance and morphology after intracerebroventricular injection in rats. AJNR Am J Neuroradiol *17*, 365-373.

Requena, T., Espinosa-Sanchez, J.M., Cabrera, S., Trinidad, G., Soto-Varela, A., Santos-Perez, S., Teggi, R., Perez, P., Batuecas-Caletrio, A., Fraile, J., *et al.* (2014). Familial clustering and genetic heterogeneity in Meniere's disease. Appl Clin Genet *85*, 245-252.

Rogosnitzky, M., and Branch, S. (2016). Gadolinium-based contrast agent toxicity: a review of known and proposed mechanisms. Biometals *29*, 365-376.

Runge, V.M., Ai, T., Hao, D., and Hu, X. (2011). The developmental history of the gadolinium chelates as intravenous contrast media for magnetic resonance. Invest Radiol *46*, 807-816.

Salt, A.N., and Plontke, S.K. (2010). Endolymphatic hydrops: pathophysiology and experimental models. Otolaryngol Clin North *43*, 971-983.

Salt, A.N., and Rask-Andersen, H. (2004). Responses of the endolymphatic sac to perilymphatic injections and withdrawals: evidence for the presence of a one-way valve. Hear Res *191*, 90-100.

Santos-Sacchi, J. (1991). Reversible inhibition of voltage-dependent outer hair cell motility and capacitance. J Neurosci *11*, 3096-3110.

Sater, A.K., and Moody, S.A. (2017). Using Xenopus to understand human disease and developmental disorders. genesis *55*, e22997.

Schmitt, S.M., Gull, M., and Brandli, A.W. (2014). Engineering Xenopus embryos for phenotypic drug discovery screening. Adv Drug Deliv Rev *69-70*, 225-246.

Schubert, M.C., and Minor, L.B. (2004). Vestibulo-ocular physiology underlying vestibular hypofunction. Physical therapy *84*, 373-385.

Schuenke, M., Schulte, E., and Schumacher, U. (2010). Thieme Atlas of Anatomy: Head and Neuroanatomy, 1 edn (Stuttgart: Thieme).

Schünke, M. (2011). Prometheus - LernAtlas der Anatomie, 3 edn (Stuttgart [u.a.]: Thieme).

Sherry, A.D., Caravan, P., and Lenkinski, R.E. (2009). A primer on gadolinium chemistry. Journal of magnetic resonance imaging : J Magn Reson Imaging *30*, 1240-1248.

Sieber, M.A., Lengsfeld, P., Frenzel, T., Golfier, S., Schmitt-Willich, H., Siegmund, F., Walter, J., Weinmann, H.J., and Pietsch, H. (2008). Preclinical investigation to compare different gadolinium-based contrast agents regarding their propensity to release gadolinium in vivo and to trigger nephrogenic systemic fibrosis-like lesions. Eur Radiol *18*, 2164-2173.

Snow, J.B., Wackym, P.A., and Ballenger, J.J. (2009). Ballenger's otorhinolaryngology : head and neck surgery (Shelton, Conn.; Hamilton, Ont.; London: People's Medical Pub. House/B C Decker).

Stengel, D., Zindler, F., and Braunbeck, T. (2017). An optimized method to assess ototoxic effects in the lateral line of zebrafish (Danio rerio) embryos. Comp Biochem Physiol C Toxicol Pharmacol *193*, 18-29.

Suzuki, H., Teranishi, M., Naganawa, S., Nakata, S., Sone, M., and Nakashima, T. (2011). Contrast-enhanced MRI of the inner ear after intratympanic injection of meglumine gadopentetate or gadodiamide hydrate. Acta Otolaryngol *131*, 130-135.

Takumida, M., Kubo, N., Ohtani, M., Suzuka, Y., and Anniko, M. (2005). Transient receptor potential channels in the inner ear: presence of transient receptor potential channel subfamily 1 and 4 in the guinea pig inner ear. Acta Otolaryngol *125*, 929-934.

Tanaka, H., Tanigawa, T., Suzuki, M., Otsuka, K., and Inafuku, S. (2010). Effects of MRI contrast agents (Omniscan) on vestibular end organs. Acta Otolaryngol *130*, 17-24.

Tillmann, B.N. (2010). Atlas der Anatomie des Menschen. In Springer-Lehrbuch (Springer Berlin Heidelberg).

Tyrrell, J.S., Whinney, D.J., Ukoumunne, O.C., Fleming, L.E., and Osborne, N.J. (2014). Prevalence, associated factors, and comorbid conditions for Meniere's disease. Ear Hear *35*, e162-169.

Wallingford, J.B., Liu, K.J., and Zheng, Y. (2010). Xenopus. Ear Hear *20*, R263-264.

Wheeler, G.N., and Brandli, A.W. (2009). Simple vertebrate models for chemical genetics and drug discovery screens: lessons from zebrafish and Xenopus. Dev Dyn *238*, 1287-1308.

Yamazaki, M., Naganawa, S., Tagaya, M., Kawai, H., Ikeda, M., Sone, M., Teranishi, M., Suzuki, H., and Nakashima, T. (2012). Comparison of Contrast Effect on the Cochlear Perilymph after Intratympanic and Intravenous Gadolinium Injection. AJNR Am J Neuroradiol *33*, 773-778.

Yang, X.C., and Sachs, F. (1989). Block of stretch-activated ion channels in Xenopus oocytes by gadolinium and calcium ions. Science (New York, NY) *243*, 1068-1071.

Zou J, P.I., Yoshida T, Gurkov R, Shi H, Li Y, et al. (2015). Milestone Research on Meniere's Disease by Visualizing Endolymphatic Hydrops Using Gadolinium-Enhanced Inner Ear MRI and the Challenges in Clinical Applications. Austin J Radiol *2(6)*, 1035.

Zou, J., Poe, D., Bjelke, B., and Pyykko, I. (2009). Visualization of inner ear disorders with MRI in vivo: from animal models to human application. Acta Otolaryngol Suppl, 22-31.

Zou, J., Poe, D., Ramadan, U.A., and Pyykko, I. (2012). Oval window transport of Gd-dOTA from rat middle ear to vestibulum and scala vestibuli visualized by in vivo magnetic resonance imaging. Ann Otol Rhinol Laryngol *121*, 119-128.

Zou, J., Zhang, W., Poe, D., Zhang, Y., Ramadan, U.A., and Pyykko, I. (2010). Differential passage of gadolinium through the mouse inner ear barriers evaluated with 4.7T MRI. Hear Res *259*, 36-43.

8 APPENDICES

8.1 Abbreviations

%	percent
~ (tilde)	approximately
<	smaller than
>	bigger than
°C	degree Celsius
3D	three-dimensional
3D-FLAIR	three-dimensional fluid attenuated inversion recovery
3D-IR TSE	three-dimensional inversion-recovery turbo spin echo
µg	microgram
µl	microliter
µM	micromolar
µm	micrometer
µmol	micromol
ABR	auditory brainstem response
ANOVA	analysis of variance
$CaCl_2$	calcium chloride
cm	centimeter
Cl^-	chloride ion
dB	decibel (a logarithmic unit of measurement in acoustics)
DMSO	dimethylsulfoxide
DNA	deoxyribonucleic acid
e.g.	for example (Latin "*exempli gratia*")
EC_{50}	effective concentration at 50%
ELH	endolymphatic hydrops
EMA	European Medicines Agency
FDA	Food and Drug Administration (US)
F	fluorescent intensity
FITC	Fluorescein isothiocyanate
FM1-43FX	n-(3-aminopropyldiethylammoniumpropyl)-4-(dibutylamino)-styryl
g	gram
ga	gauge
GBCA	gadolinium-based contrast agent
Gd^{3+}	gadolinium ion
h	hour
H^+	proton
HCl	hydrochloric acid
HCO_3^-	hydrogencarbonate
H_2O	water
hCG	human chorionic gonadotropin
HEPES	4-(2-hydroxyethyl)-1-piperazineethanesulfonic acid

hpf	hours post fertilization
H_2SO_4	sulfuric acid
i.t.	intratympanic
i.v.	intravenous
IU	international units
K^+	potassium ion
KCl	potassium chloride
kg	kilo gram
kHz	kilo hearts (frequence)
K_{cond}	conditional stability constant
K_{therm}	thermodynamic stability constant
l	liter
LC_{50}	lethal concentration at 50%
logP	partition-coefficient
M	molar
MD	Meniere's Disease
MET channel	mechanoelectrical transtuction channel
Mg^{2+}	magnesium ion
$MgSO_4$	magnesium sulfate
mg	milligram
ml	milliliter
mm	millimeter
mmol	millimol
MMR	Marc's modified ringer solution
MRI	Magnetic Resonance Imaging
mV	millivolt
n	number
Na^+	sodium ion
NaCl	sodium chloride
NaOH	sodium hydroxide
N.D.	not determined
ng	nanogram
nm	nanometer
NSF	Nephrogenic systemic fibrosis
PBS	phosphate buffered saline
pH	decimal logarithm of the reciprocal of the hydrogen ion activity in a solution
R	rest / moiety
RFU	relative fluorescent unit
SD	standard deviation
sec	second
T	Tesla
$T_{1/2}$	Dissociation half-time at pH 1.0 and 25°C
TRPV4	TRP vanilloid 4 channel
VOR	vestibular ocular reflex
vs.	versus
x	fold
σ	standard deviation

8.2 List of Tables

8.3 List of Figures

8.4 Publications and Scholarships

·   Scholarship, poster presentation and abstract publication at the 86th Annual Meeting of the German Society of Oto-Rhino-Laryngology, Head and Neck Surgery in Berlin, Germany, May 2015.

   Eichel V, et al. Assessment of hair cell toxicity of gadolinium-based contrast agents in Xenopus laevis embryos. 86th Annual Meeting of the German Society of Oto-Rhino-Laryngology, Head and Neck Surgery. Düsseldorf: German Medical Science GMS Publishing House; 2015. Doc15hno02

·   Poster presentation at the 1st nationwide *Xenopus*-Meeting in Hohenheim, Germany, October 2013.

9 ACKNOWLEDGEMENTS